Review

Overview on Permanent Magnet Motor Trends and Developments

Vasileios I. Vlachou , Georgios K. Sakkas , Fotios P. Xintaropoulos , Maria Sofia C. Pechlivanidou , Themistoklis D. Kefalas , Marina A. Tsili , Antonios G. Kladas *

Posted Date: 22 December 2023

doi: 10.20944/preprints202312.1678.v1

Keywords: Permanent-Magnets; Electric Vehicles; Electric Motor; Demagnetization; Geometry Optimization; Constraint Model, Finite Elements Analysis; Short Circuit; Neodymium Magnets; Parameter Sensitivity Analysis

Review

Overview on Permanent Magnet Motor Trends and Developments

Vasileios I. Vlachou , Georgios K. Sakkas , Fotios P. Xintaropoulos , Maria Sofia C. Pechlivanidou , Themistoklis D. Kefalas , Marina A. Tsili , Antonios G. Kladas *

Posted Date: 22 December 2023

doi: 10.20944/preprints202312.1678.v1

Keywords: Permanent-Magnets; Electric Vehicles; Electric Motor; Demagnetization; Geometry Optimization; Constraint Model, Finite Elements Analysis; Short Circuit; Neodymium Magnets; Parameter Sensitivity Analysis

 doi:10.20944/preprints202312.1678.v1

Review

Overview on Permanent Magnet Motor Trends and Developments

Vasileios I. Vlachou [1], Georgios K. Sakkas [1], Fotios P. Xintaropoulos [1] Maria Sofia C. Pechlivanidou [1], Themistoklis D. Kefalas [2], Marina A. Tsili [3] and Antonios G. Kladas [1,*]

[1] Laboratory of Electrical Machines and Power Electronics, School of Electrical and Computer Engineering, National Technical University of Athens, 15780, Athens, Greece; vasilvlachou@mail.ntua.gr; gsakkas@mail.ntua.gr; fotisxintaropoulos@hotmail.com; mariasofiapech@mail.ntua.gr

[2] Hellenic Electricity Distribution Network Operator HEDNO S.A., 10434, Athens, Greece; t.kefalas@deddie.gr

[3] Independent Power Transmission Operation (IPTO-ADMIE), 89 Dyrrachiou Str., 15343, Athens, Greece; MTsili@admie.gr

* Correspondence: kladasel@central.ntua.gr; Tel.: +30-210-7723-765

Abstract: The extreme environmental issues and the resulting needs to save energy have turned the attention to electrification of energy applications. One of the key components involved in energy efficiency improvements is the appropriate conception and manufacturing of electric machines. This paper overviews the electromagnetic analysis governing the behavior of permanent magnets that enabled substantial efficiency gains in recent electric machine developments. Particular emphasis is given to model the properties and losses developed in permanent magnets in the emerging high speed applications. In addition, the investigation of properties and harmonic losses related to ferromagnetic materials constituting the machine magnetic circuits are equally analyzed and discussed. The experimental validation of the implemented methodologies and developed models with respect to the obtained precision is reported. The introduction of mixed numerical techniques based on the finite element method intended to appropriately represent the different physical phenomena encountered is outlined and discussed. Finally, fast and accurate simulation techniques including aggregated lumped parameter models considering harmonic losses associated with inverter supplies are commented.

Keywords: Permanent-Magnets; Electric Vehicles; Electric Motor; Demagnetization; Geometry Optimization; Constraint Model; Finite Elements Analysis; Short Circuit; Neodymium Magnets; Parameter Sensitivity Analysis

1. Introduction

Electric vehicles represent an emerging application in the field of transportation electrification initiatives. Leading automotive manufacturers have committed to producing electric vehicles to replace internal combustion machines. Some of the key factors that have led to this change are related to reduced environmental emissions and fuel efficiency [1]. Furthermore, one of the key advantages is the energy saving capabilities related to the appropriate propulsion system, namely concerning the battery, inverter, and electrical motor. Primarily in electrification applications, permanent magnet electric motors are the primary technology in most applications due to their increased efficiency [2].

The rapid development of permanent magnet (PM) materials during the last decades enabled the design of high-performance permanent magnet synchronous motors (PMSMs), which are preferred by many electric vehicle (EV) manufacturers [3]. The high efficiency, the low maintenance required and the high power/torque density achieved are their main attractive characteristics. Some additional advantages of using permanent magnet motors include power factor improvement, better dynamic performance and higher reliability when compared to rival types of electric motors [4].

 doi:10.20944/preprints202312.1678.v1

However, the PMSMs designers and manufacturers have to meet many challenges during the PMSMs production process. For instance, more complex control strategies are required, while the flux-weakening technique, which is employed under high-speed driving, increases the risk of PMs demagnetization. The rare-earth PMs may suffer from high eddy current losses in particular in high-speed applications and their manufacturing imperfections may affect negatively the machine's electromagnetic behavior. Also, the vibrations of the traction system may be significant since the PMs introduce strong magnetic forces. That is why, the EV/HEV system's reliability and fault tolerance have to be considered during the PMSMs design procedure [5].

The evolution of power electronic converters in combination with the application of appropriate control techniques has positioned permanent magnet motors as a promising and favored technology that addresses key features of modern electric vehicles as well as high speed applications. The basic purpose of this paper is to provide a survey of various contemporary machine topologies, with a particular emphasis on different permanent magnet configurations developed, compared in Section 2. In Section 3, the literature survey focuses, on material properties and experimental results, examining characteristics including losses and in particular harmonic losses at higher speeds originated from inverter supplies. In addition, the results obtained from experimental setups for various types of permanent magnet configurations are analyzed and discussed; to that respect, magnetic circuits of electric machines with surface mounted magnets on the rotors are considered, and the effects on the losses due to epitaxial placement on the surface of the magnets of suitable micro-layers with ferromagnetic and/or conducting material grains are investigated. It should be noted that, during the experimental validation of the characteristics of the permanent magnets, it was shown that it was necessary to investigate them in conjunction with the characteristics of the magnetic laminations in presence of the permanent magnets; to that respect, iron lamination losses measured in standard gapless magnetic circuits such as Epstein and toroidal cores do not provide sufficient accuracy in regions neighboring permanent magnets, while C-Core type magnetic circuits under coexistence of DC and AC excitations enable good precision in harmonic loss prediction. In addition, appropriate models for synchronous permanent magnet motor analysis under three-phase short-circuit conditions enabling consideration of magnet demagnetization risks are presented in Section 4. Section 5, is devoted to numerical methodologies using mixed numerical techniques based on finite element method proposed to facilitate permanent magnet motor analysis. Moreover, lumped parameter equivalent circuit models accounting for harmonic losses through consolidated parameters are reported in Section 6. Section 7 mentions potential impact of rotor mechanical deformation on permanent magnet motor characteristics. Finally, the basic conclusions derived from the literature survey on permanent magnet motors and the respective application trends are summarized in Section 8.

2. Topologies of Permanent Magnet Rotors

2.1. Inner and Outer Rotor Configurations

To satisfy the above requirements, numerous PMSMs alternatives have been introduced in the literature. Expert of the various stator windings configurations, there are several rotor design variants, too. The rotor can be either inner or outer with respect to the stator's position. The inner topology is more commonly used since it guarantees the achievement of a value for the airgap flux density amplitude close to the PMs magnetic flux density, enables a wider speed range operation and concludes to satisfactory flux-weakening capability. The above features deteriorate when an outer-rotor structure is adopted. For such a motor, the temperature alleviation is not an easy task as the stator winding coils (whose copper losses are usually the major heat source) are placed at the inner part of the machine. Due to the poorer temperature alleviation, the researchers have focused on the development of advanced cooling systems [6]. On the contrary, the winding coils assembly is much easier as the stator teeth points outwards. Furthermore, the motor's axial length can be smaller. A high value is frequently assigned to the outer diameter to axial length ratio. This benefits substantially the torque density. The outer-rotor PMSM's net mass may be up to 15% smaller than the

 doi:10.20944/preprints202312.1678.v1

corresponding one of a motor with inner rotor [7]. The outer rotor motors are the primary choice in electrified applications as they reduce transmission losses both during propulsion and regenerative braking. However, they require suitable and precise design as the high torque requirements must allow the vehicle to start on uphill roads in order to achieve the necessary speed. At the same time, the higher moment of inertia contributes to the vibrations and torque harmonics mitigation. For the above reasons, the outer–rotor PMSMs are the dominant structure at the in-wheel electrified systems. The high-speed operation is not a great challenge for this machine since the centrifugal forces retain the PMs [8].

2.2. Sourface-Mounted Permanent Magnet Rotors

Concerning the magnets' placement, there is another classification for the PMSMs. In particular, they are divided into: a) surface-mounted (SPMSMs) and b) interior (IPMSMs) PMSMs. In the first case, the PMs are attached on the rotor's (inner or outer circumference) and they are magnetized radially. The motor's effective airgap length is equal to the sum of the PM's height and the actual airgap length since the magnetic permeability of the PMs is comparable to that of the air. The large effective airgap length decreases the motor's self-inductance. The tooth tip leakage inductance and thus the total inductance can be increased through the appropriate stator teeth design for a better fault-tolerance capability. The PMs of a SPMSM are exposed directly to the armature reaction field due to their position. So, there is high risk for them to be susceptible to partial irreversible demagnetization. This can be avoided thanks to a sleeve (made of non-ferromagnetic material with high electrical conductivity) that is placed around them [9].

The sleeve helps also the magnet's retention when the motor's rotational speed is too high. The rotor of a SPMSM has no saliency. The SPMSM's efficiency is high as a large amount of magnetic flux is concentrated in the airgap. Its flux-weakening capability is reduced and its overload capability can be regarded as satisfactory. The permeance variation in the airgap may cause high torque ripple when the PMs and the stator teeth dimensions are not properly selected. The curving of the magnets' surface declines the torque ripple, but this is a countermeasure of high cost [10].

The so far research works (targeting either to enhance the SPMSM's performance or to mitigate its inherent undesirable features) deal with the following topics: a) the examination of different PMs shapes and segments number; b) the demagnetization analysis of the SPMSMs; c) the study of the impact of poles/slots combination on the SPMSM's operational characteristics; d) the development of advanced analytical models/methods for the motor's electromagnetic performance estimation as well as its thermal behavior prediction; e) the introduction of novel design methodologies, especially for SPMSMs with high-speed operation and/or outer-rotor topology and f) the incorporation of artificial intelligence based methods on the design process. The recent advances in the SPMSMs design and analysis are presented and discussed at the next paragraphs of this Section.

Regarding the magnet's geometry, the authors of [11] proposed an analytical method, based on Schwarz-Christoffel mapping, for PMs shape optimization of an asymmetrical and unidirectional 12-poles SPMSM. According to the applied technique, the PMs were divided into finite cells so that each cell can be assigned with either air (off) or magnet (on). The optimization problem was solved by using genetic algorithm (GA). The results, obtained through 2-D and 3-D finite element analysis (FEA) simulations demonstrated that the asymmetrical magnet shape deteriorates substantially the motor's cogging torque and torque ripple, while simultaneously increases slightly the average output torque. In [12], four different magnet shapes (illustrated in Figure 1) were analyzed and compared to each other for a SPMSM with full-pole-pitched distributed stator winding.

 doi:10.20944/preprints202312.1678.v1

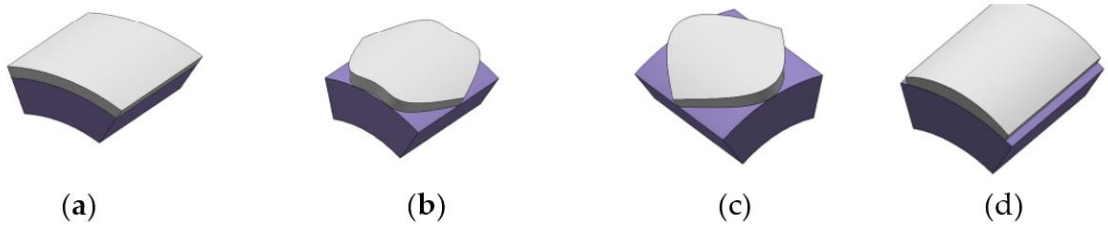

Figure 1. The PMs designs examined in [11]: (**a**) rectangular-shaped; (**b**) butterfly-shaped; (**c**) egg-shaped; (**d**) bread-load-shaped magnet.

As it can be seen from Figure 1, the thickness of the proposed PM is uniform along the radial direction so as not to impair the magnet's ability to handle the demagnetization force. The introduced shaped-magnet design was proven to have clear advantages over the rest tested topologies since it: a) delivers the same amount of torque, but with almost zero torque ripple even at high electric loading and b) uses more efficiently the PMs material. Overall, it was concluded that the specific shaping technique is suitable for the design of high-performance SPMSMs as it has not negative impact on the motor's average output torque.

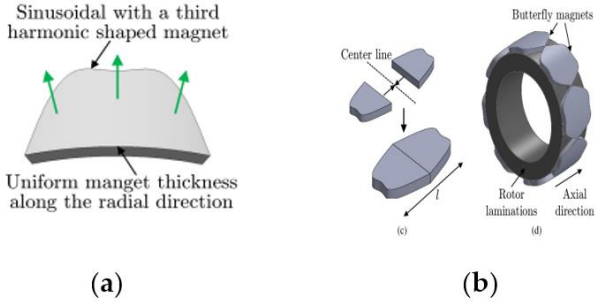

Figure 2. The PM design concept proposed in [11]: (**a**) sinusoidal plus third harmonic shaped PMs; (**b**) proposed rotor design with butterfly-shaped PMs.

A study with similar research objectives was concluded in [13], where a novel design method for the pole shape formation was developed by adopting a cycloid curve. The calculated results were quite consistent with FEA and experimental results. The effect of different PM shapes (depicted in Figure 3) on the SPMSM's cogging torque was highlighted in [14] aiming to identify the optimal design for each one. In order to overcome the limitations (which come as a result of the low versatility of the motor PMs fabrication technologies) on the development of new rotor geometries, the cold spray additive manufacturing was employed in [15] for shaping the magnets of a radial-flux inner-rotor SPMSM.

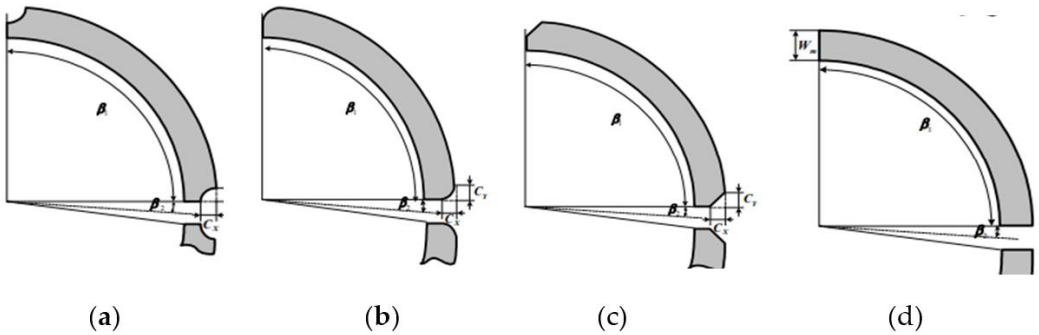

Figure 3. The different PM shapes examined in [14]: (**a**) Description of what is contained in the first panel; (**b**) Description of what is contained in the second panel.

 doi:10.20944/preprints202312.1678.v1

The magnets have been shaped according to a sinusoid along the axial direction while them thickness has been kept uniform along the radial direction. The performance of the machine with sinusoidal shaped rotor was found to be superior to that of a conventional rectangular shaped rotor design when the flux leakage, output torque, cogging torque and back-electromotive force (Back-EMF) were examined. The influence of the PMs segmentation on the aforementioned motor's operational features was studied in for different slots/poles combinations and valuable conclusions were drawn. As for the PMs demagnetization, the impact of three-phase short-circuit currents on the SPMSM's performance under different load conditions was studied in. Moreover, a novel methodology, which takes into account the edge effect of SPMSMs, was introduced in for the demagnetization analysis of ferrite PMs [16]. Since the PMs shape and dimensions are not the only parameters that affect the motor's cogging torque and torque ripple, the proper selection of stator teeth dimensions and poles/slots combination is necessary, too. Such investigations were conducted in [17] and [18] toward the SPMSM's vibration and losses minimization.

2.3. Interior Permanent Magnet Rotors

As already mentioned, the second category of the PMSMs are the IPMSMs, whose PMs are either inset or embedded into the rotor laminations are they are either tangentially or radially magnetized. Their most important advantages are greater resistance to PMs as well as better shielding against demagnetization. They are salient-pole machines. Their d-axis inductance is lower than that in q-axis. The saliency ratio and the resulted reluctance torque of the IPMSMs with buried PMs are highly dependent on: a) the PMs dimensions, position and configuration and b) the flux barriers location and geometry [19]. Special attention has to be paid to the flux barriers design parameters determination since they have great impact on the motor's electromagnetic performance. As for IPMSMs design methodology of flow barriers it was found that they can reduce core losses in both stator and rotor. Symmetrical and asymmetrical flow barriers were considered. In the first case it was found that they have different shapes (trapezoidal, triangular, etc.) and are placed at both ends of PMs in order to regulate and guide the magnetic flux around the rotor poles. Conversely, in the second case, they may have a different geometric configuration and orientation on the both sides of the permanent magnets, while they may exist only at one side of the rotor pole.

By optimizing the design of the flux barriers, enhancement of the torque capacity of IPMSMs, reduction of the torque ripple and minimizing the risk of irreversible demagnetization of PMs can be achieved. Thus, based on the findings of [20], it can be concluded that large flux barriers with smaller angle are preferable when rare earth magnets are used in the magnets. Considering the case of ferrite PMs, we find that the design of flow barriers is not appropriate as extended torque pulses can be occurred, creating significant problems in machine operation. Regarding the stator winding configuration, either distributed or concentrated windings can be utilized. However, the distributed windings enable the more sufficient exploitation of the IPMSM's reluctance torque [21]. The electromotive force, induced by the PMs, of the IPMSMs is lower compared to that of the SPMSMs. Concerning the efficiency, the IPMSMs have clear advantage over the SPMSMs at high speeds, while at low speeds their performance is inferior [22]. Their high torque density levels along with their ability to handle a wide operation range with deep flux-weakening control make them the leading candidates for EVs [23]. Howbeit, their design process is characterized by increased complexity due to the large number of design variables [24]. Notwithstanding that, numerous rotor geometries have been analyzed, prototyped and evaluated by taking into account features, such the efficiency, flux-weakening-capability, particular losses, thermal behavior, overload capability, manufacturing cost, risk of failure, etc. [25].

A design variation of the SPMSMs, the inset PMSMs, is depicted in Figure 4a. The PMs are allocated on the rotor's circumference and the gaps among them are filled with the core's soft ferromagnetic material. In this way, a better restraint of the PMs is achieved. Nonetheless, their thermal behavior is poorer as: a) less circulating air surrounds the magnets and b) high iron losses appear close to them. The rotor's hysteresis losses increase since the ferromagnetic material among the PMs is easily saturated. The rotor of this machine is anisotropic as the iron's relative magnetic

 doi:10.20944/preprints202312.1678.v1

permeability is much higher than that of the PMs [26]. The difference between the q- and d-axis inductances creates reluctance torque. Thus, the operating principle of the inset PMSM is similar to that of the IPMSMs with buried PMs.

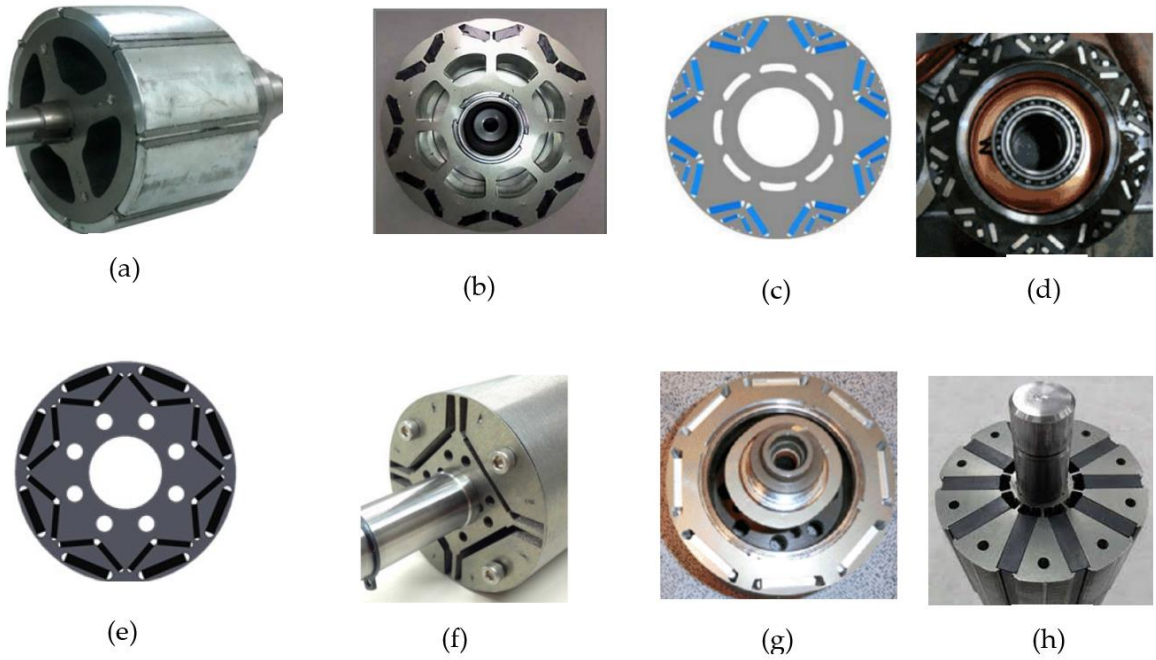

Figure 4. PMSM rotor topologies: (**a**) inset; (**b**)-(h) buried PMSMs.

A design variation of the SPMSMs, the inset PMSMs, is depicted in Figure 4a. The PMs are allocated on the rotor's circumference and the gaps among them are filled with the core's soft ferromagnetic material. In this way, a better restraint of the PMs is achieved. Nonetheless, their thermal behavior is poorer as: a) less circulating air surrounds the magnets and b) high iron losses appear close to them. The rotor's hysteresis losses increase since the ferromagnetic material among the PMs is easily saturated. The rotor of this machine is anisotropic as the iron's relative magnetic permeability is much higher than that of the PMs [26]. The difference between the q- and d-axis inductances creates reluctance torque. Thus, the operating principle of the inset PMSM is similar to that of the IPMSMs with buried PMs.

Among the most important decisions during the design the during the design stage is the selection of the iron bridges size as it affects substantially the IPMSM's back-emf and the magnetic flux leakage [27]. The findings of [28] indicated that the d-axis inductance varies with the iron bridges saturation level.

The findings of [29] indicated that the d-axis inductance varies with the iron bridges saturation level. The relationship between the rotor geometry and the trade-offs required for the motor's wide speed range operation was investigated at the above research work, too. The incorporation of bypass ribs outspreads the IPMSM's constant power region and boosts its flux-weakening capability [22]. Also, the minimum thickness of the bridges is imposed by mechanical constraints. The maximum mechanical stress on the iron bridges for various angles between the PMs has been estimated in [30] through an analytical method. The mechanical stress is alleviated when the flux barrier corners are rounded. The optimal design of the rotor's iron bridges and flux barriers is essential for the IPMSM's performance improvement. This can be implemented either by conducting a sensitivity analysis [31] or by following an optimization-based finite element analysis approach.

Another design parameter of great importance is the rotor rib, i.e., the distance between the flux barrier and the rotor circumference. The IPMSM's maximum output power variation as a function of the specific dimension was thoroughly studied in [32]. As the rotor rib becomes larger, the stress concentration is relieved at high speeds, but the IPMSM's performance deteriorates. The opposite

 doi:10.20944/preprints202312.1678.v1

happens when the rib thickness gets smaller values. Additionally, the rib thickness affects the d- and q-axis inductances and consequently the flux-weakening operation. The angle between the PMs is subjected to constraints, too. The V-shaped rotor is not easily applicable when the poles number is large as there is less available space for the PMs. In this case, the angle between the PMs decreases. For low angle values, the rotor core's material is saturated and higher rotor losses occur as highlighted in [33]. The motor's performance at the constant power region is negatively affected for low angle values, too.

On the other hand, the rotor losses become lower as the angle value gets higher. Another defect of the V-shaped IPMSM is the fact that the airgap magnetic flux density distribution is less sinusoidal. It contains harmonics of high order than cause torque ripple, vibrations and noise. The harmonics can be reduced through the appropriate choice of the pole arc to pole pitch ratio. The effect of the specific design variable on the airgap magnetic flux density and back-emf was analyzed and discussed in [34] and [35]. Another effective design solution is the PMs shifting. It leads to the cogging torque and torque ripple suppression, while the average output torque is preserved [36]. Toward the specific direction, the impact of stator slotting and armature reaction field was studied in [37] for IPMSMs with multi-segmented skewed poles. Guidelines regarding the proper poles/slots combination choice were provided in [38] for IPMSMs with fractional-slot concentrated winding (FSCW).

The aim of these research effects was to establish a base capable of securing the reliability of the IPMSMs that are used at traction applications. In order to overcome few of the V-shaped rotor IPMSMs inherent defects, the double-V structure (illustrated in Figure 4(c)) has been introduced. An indicative alternative design is shown in Figure 4(d). The manufacturing complexity of this rotor is greatly increased compared to that of an IPMSM with single magnet per pole. The topology of Figure 4(e) is known as delta-shaped rotor. It has three PMs per pole that are arranged in two layers. The first layer contains two magnet blocks that create a V-shaped structure. The second layer includes only one straight magnet block. The difference between the q- and d-axis inductance of this motor is very high. Although a high reluctance torque is produced, this torque can be hardly utilized due to the DC link voltage limit. So, it has moderate field-weakening capability. Its torque density is slightly higher than that of the single V-shaped rotor. In order to boost even more the power/torque density of the delta-shaped rotor IPMSM, the Hairpin windings was preferred in [39]. The U-shaped rotor is depicted in Figure 4(f). At this geometry, the layout of letter "U" is built by the PMs. A PMs volume smaller than the corresponding one of the V-shaped rotor IPMSM is required aiming the motor to deliver the same output torque. Due to its satisfactory torque capability, many already published research works deal with the analysis and design of this IPMSM.

The rectangular-type rotor is presented in Figure 4g. It has one PM block per pole. Its PMs are radially magnetized and embedded near the rotor surface. The manufacturing process of this topology is quite easy. The PMs are well protected against the centrifugal forces and the armature reaction field. Howbeit, the PMs suffer from much higher eddy current losses compared to the rest IPMSMs due to the larger magnet poles cross-sectional area. Therefore, the PMs segmentation is demanded. Another drawback of the specific rotor design is the high leakage of flux through the iron bridges [40]. Its flux-weakening capability can be characterized as satisfactory according to the findings. Many research efforts gave emphasis on the torque quality improvement. A thorough analysis was performed in [41] regarding the impact of PM segments numbers and geometrical parameters on the torque characteristics. It was found that increasing the PM's thickness instead of its width is more beneficial for the torque. Significant reduction of the torque ripple was achieved in [42] by conducting a range analysis on data from orthogonal experiments.

The spoke-type rotor is illustrated in Figure 4h. The PMs are of rectangular shape and they are tangentially magnetized and inserted in deep slots. The rotor geometry permits the magnetic flux concentration. When the magnet bridges are avoided, the flux moving inside the rotor from one to pole to the adjacent one is averted [43]. The effect of both bridge leakage and axial leakage was considered in during the design process of an IPMSM of this type. The magnetic flux concentration leads to an airgap magnetic flux density value higher than that of the PMs. This feature is of great

 doi:10.20944/preprints202312.1678.v1

importance since the produced reluctance torque is low [44]. The rotor's manufacturing is easy and of low cost. The restricted field-weakening capability and the back-emf distortion are the utmost disadvantages of this IPMSM. A novel design method was proposed in [45] toward the minimization of cogging torque and torque ripple without proceeding to the PMs skewing. Asymmetric flux barriers were used along with the inverting lamination technique.

The optimization of the rotor shape in [46] was found to be effective enough. The torque ripple was reduced while the average torque remained unaffected. A novel structure with hybrid radial and axial flux-concentrating capability was presented in [47] to reduce the interpolar leakage flux. The electromagnetic performance of the developed model was superior compared to that of a traditional spoke-type IPMSM. Targeting the efficiency enhancement, a comparative analysis was made in [48] for IPMSMs whose cores were made of a dual phase magnetic material and conventional ferromagnetic materials for rotor laminations.

Expect from the so far described rotor designs, there is an adequate number of alternative topologies in the literature. They are either design variations of the conventional rotors or combinations of them, while few of them exhibit unique geometrical and operational characteristics. In any case, the most promising ones are presented herein. The hybrid magnets rotor structure of Figure 5a is formed when: a) high-resistivity ferrite magnets are introduced in the flux paths of the d-axis and q-axis and b) V-type NdFeB PMs are placed in the d-axis path. As stated in [49], the fill of the air grooves between the tangential magnet blocks with ferrite PMs improves the torque quality and makes the airgap magnetic flux density more sinusoidal. The reduction of rotor and PMs losses was achieved by finding the optimal angle between the V-type PMs.

A new rotor shape, shown in Figure 6b, was developed in [50] especially for IPMSM's high-speed operation. The motor's electromagnetic performance was found to be superior compared to that of a SPMSM with the same specifications, while the PMs volume has been decreased by 53%. The rotor geometry of Figure 6c contains two layers of PMs (i.e., one of U-type and one of V-type). In [51], the impact of the involved rotor design variables was investigated and explained by employing both analytical and numerical techniques. The final values of the geometrical parameters were selected by considering key performance metrics, the motor's flux-weakening capability and the effect of short-circuit faults on the PMs.

In [52], a design methodology was proposed for the high-speed multi-layer rotor IPMSM of Figure 6d, which has ferrite PMs. Since the ferrite magnets have much lower coercive force than that of the NdFeB PMs, great emphasis was given to the incorporation of PMs demagnetization analysis and rotor mechanical analysis at all the design stages. Despite the fact that the outer rotor topology is more popular at the SPMSMs, there are research works that deal with the design of outer-rotor IPMSMs. The IPMSM of Figure 6e was studied in [53]. PMs of rectangular shape were allocated near the rotor's inner circumference. The motor's cogging torque and torque ripple was minimized by optimizing the flux barriers design. A hybrid double-U rotor with two-layer crescent barriers (depicted in Figure 6f was introduced in [54] aiming to maximize the IPMSM's output torque and reduce the utilization of high-cost rare-earth PMs.

Preprints.org (www.preprints.org) | NOT PEER-REVIEWED | Posted: 22 December 2023 doi:10.20944/preprints202312.1678.v1

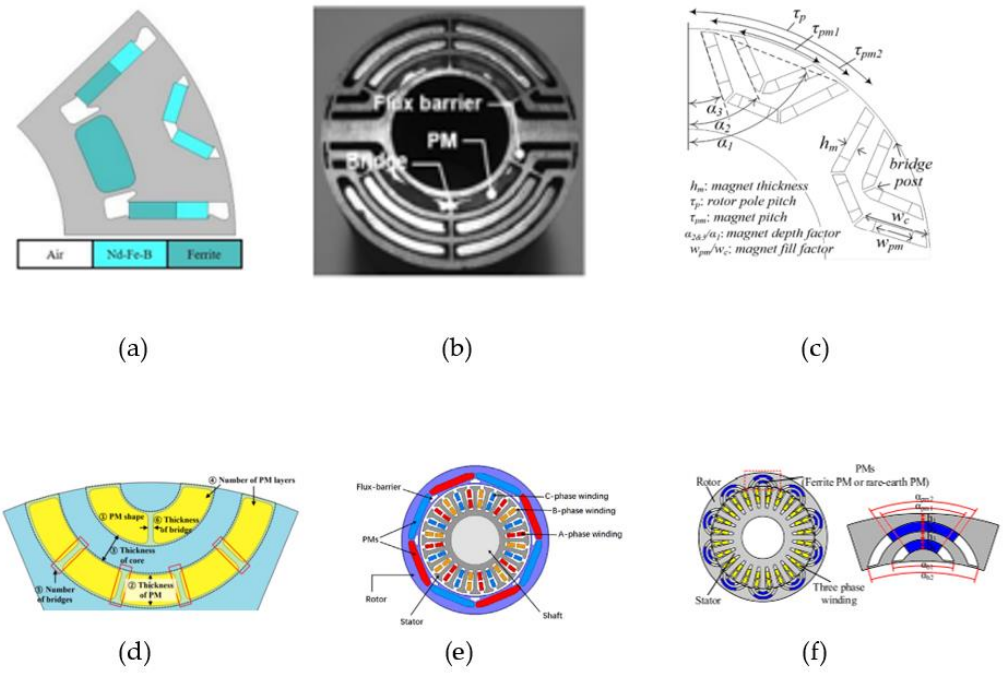

Figure 5. Promising IPMSM topologies.

2.4. Comparative Analysis of PMSMs Configurations

The performance of the V-shaped rotor IPMSM was compared to the respective one of the configurations with rectangular PMs in [55]. The PMs dimensions along with the flux barriers design were optimized aiming to meet specific requirements, while the authors of [56] estimated the rotor's stress distribution under maximum sped operation to validate its mechanical stability.

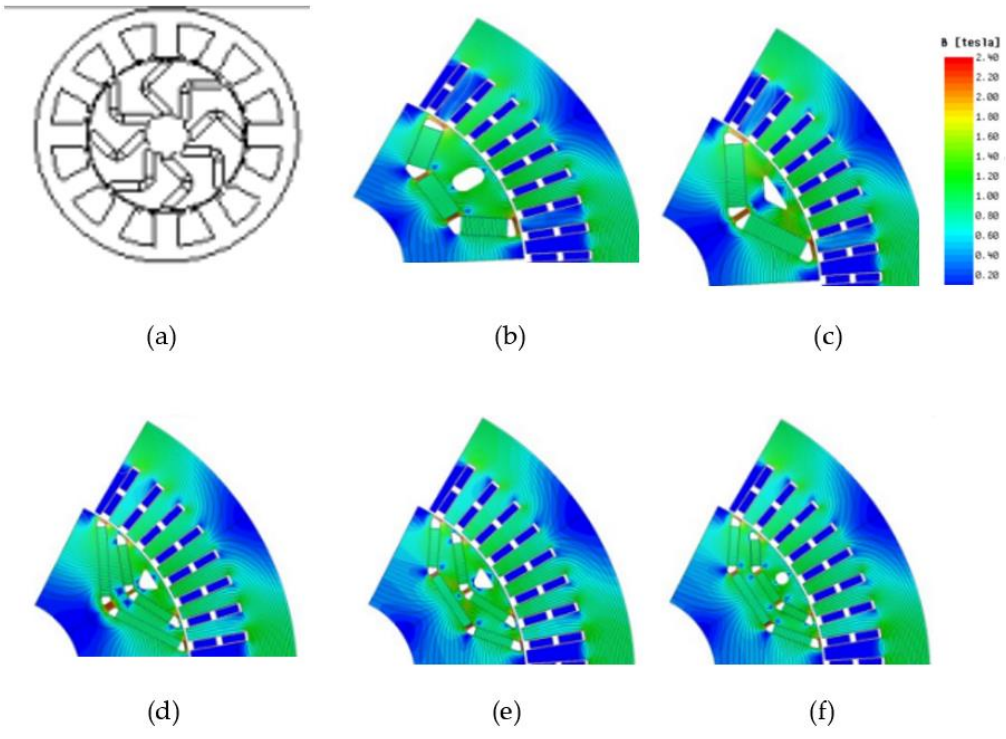

Figure 6. IPMSM topologies: (**a**) the flux-concentrated V rotor design; (**b**) V-shape; (**c**) U-shape; (**d**) VV-shape; (**e**) VU-shape; (**f**) UU-shape.

 doi:10.20944/preprints202312.1678.v1

Also, alternative rotor configurations have been analyzed and compared to the conventional ones. For instance, the topology of Figure 7b, which has PMs both radially and tangentially magnetized, was found to present higher torque capability and saliency ratio than the ones of the equally-operated spoke-type IPMSM (shown in Figure 8a. The asymmetric magnetic pole structure of Figure 8d that uses bonded rare-earth PMs achieves higher output torque compared to the rectangular-type IPMSM of Figure 8c that has sintered NdFeB PMs. In particular, its reluctance torque was increased by 34% and the total average output torque was enhanced by 6.5%, as mentioned in [57]. Its only disadvantage is the higher torque ripple, which can be reduced by optimizing the magnets layout.

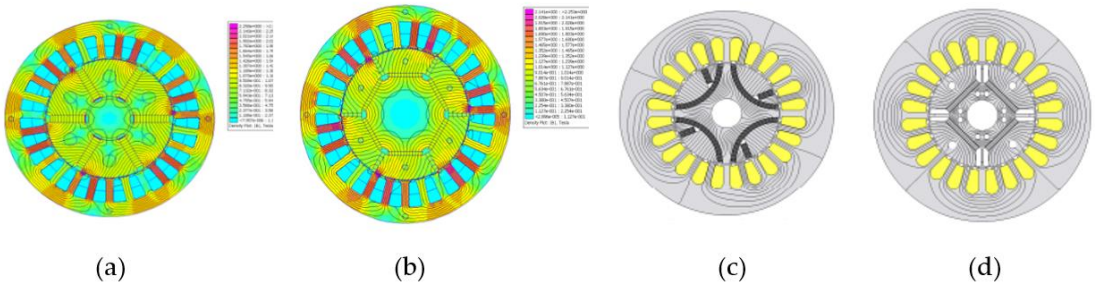

Figure 7. IPMSM topologies: (a) the spoke-type IPMSM, (b) the hybrid rotor, (c) the asymmetric magnetic pole structure and (d) the model used as a reference point.

Moreover, the configuration, depicted in Figure 6a, which is known as flux-concentrated V design was studied. From the findings of this research work, the following are observed: a) the spoke type rotor leads to the highest no-load back-emf per PM material usage while the V-type results to the lowest one; b) the back-emf total harmonic distortion of the spoke and flux-concentrated V rotor is the highest ones; and c) the aforementioned topologies have poor demagnetization characteristics.

The cross-sectional view along with the no-load magnetic flux density distribution of the final models are given in Figure 7b-f. From the obtained results, it can be noticed that: a) the double-layer PM machines have lower magnetic flux density harmonics content compared to the single-layer ones, b) the q-axis inductance of the five models in almost the same; c) the U-shape rotor motor has the largest d-axis inductance, followed by the single-V double-V, and hybrid (i.e. UV-shape) rotor, d) the U-shape arrangement has the lowest difference between the q-axis and d-axis inductance, which is quite close to that of the V-shape rotor, e) the double-layer PMs motors have almost the same difference between the d-axis and q-axis inductances and their values are higher than those of the single-layer PMs, f) the U-shape rotor has the best mechanical performance, while the V-type one has the worst one and g) the U-shaped IPMSM has the best anti-demagnetization ability among the five rotors under the three-phase symmetric short-circuit faults.

The omega-shaped PMs arrangements were proposed as substitutes of conventional rectangular-type IPMSMs to enhance the torque characteristics. The developed geometries (illustrated in Figure 9a, 9b, 9c have bonded instead of sintered PMs and exhibit: a) lower iron losses due to the lower magnetic flux density distribution, b) higher efficiency under the maximum output control, c) lower torque ripple and d) higher average output torque. Modified models of the V-type IPMSM were introduced in [58]. The IPMSM (depicted in Figure 10a of the 3rd generation Toyota Prius model was considered as the reference motor. The modified models of Figure 9b and Figure 9c were developed by applying an optimization algorithm. The motors' performance was evaluated by taking into consideration the electric vehicle's behavior under three different driving cycles.

The results revealed that the proposed modified V2 model (shown in Figure 9c) has higher torque density by 36% while the PMs volume has been decreased and significantly lower cogging torque. It leads to higher electric drive efficiency by 0.84% (in average) at the electric vehicle level for the three examined drive cycles. Its only undesirable feature is the mitigation by 14.69% of the motor's maximum output power capability.

 doi:10.20944/preprints202312.1678.v1

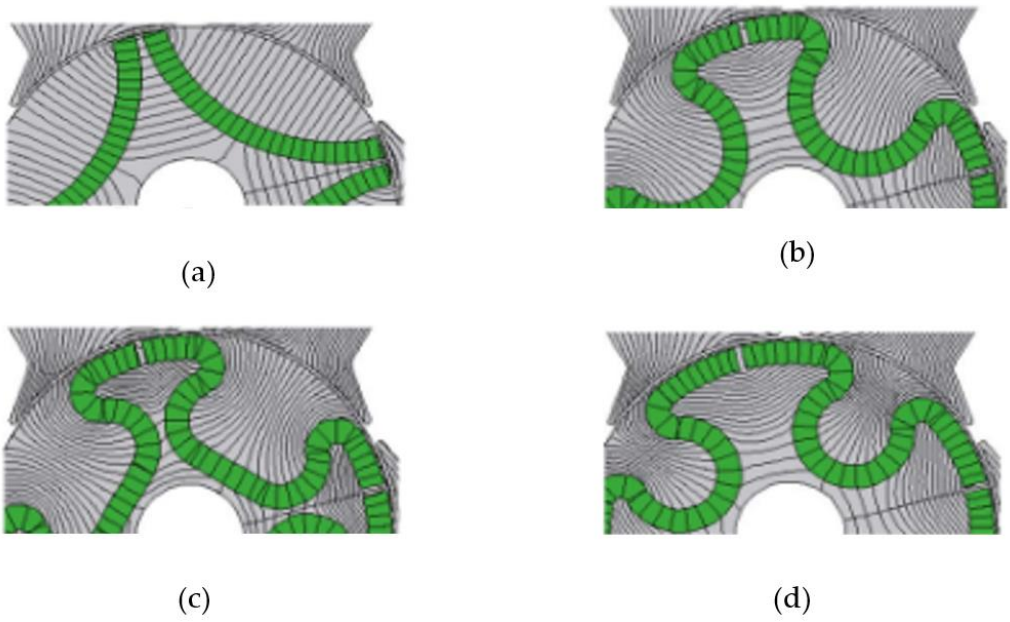

Figure 8. The omega-shaped PMs.

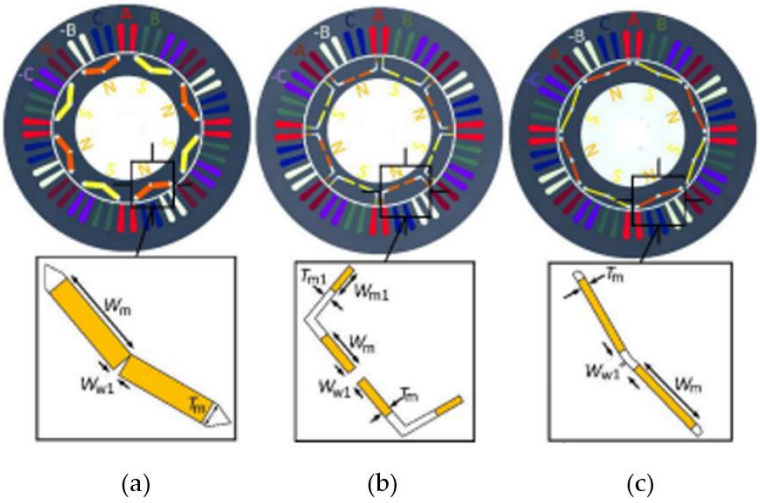

Figure 9. The PM arrangement studies in [73]: (**a**) the IPMSM of the 3rd generation Toyota Prius model, used as a reference motor; (**b**) the modified V1 model; (c) the modified V2 model.

3. Thermal Analysis and Permanent Magnet Demagnetization Effects

3.1. Magnetic Material Categories

Designing electric motors with high power density for EVs can be challenging due to power loss and temperature rise. To overcome these challenges, a significant amount of research has been conducted on the design high-density electric motors with advanced materials, improved physics and mathematics, and improved power density, modelling of the materials and the motor system, as well as interdisciplinary optimization at the system level of the of the entire drive system [59].

New manufacturing techniques have also been introduced aiming to reduce production costs such as 3-D printing. Although important magnetization levels have not been attained yet, such technologies present advantages in high speed and high supply frequency applications due to the reduced losses developed, and could constitute an attractive possibility for low-cost core production

 doi:10.20944/preprints202312.1678.v1

in such cases. The features of fabricated cores from a commercially available low-mass and low-cost magnetic polylactic acid (PLA) iron filament are under investigation [60].

Magnetic materials belong to one of the following categories: diamagnetic, paramagnetic, ferromagnetic, antiferromagnetic and ferrimagnetic.

- Diamagnetic materials have no pure magnetic moment, at the atomic or molecular level. When diamagnetic materials are subjected to the action of an external field, atomic currents are produced which cause total magnetization which opposes the external field that caused it. Bismuth (Bi) is an example of the diamagnetic material.
- Paramagnetic materials have a pure magnetic moment at the atomic level, but the coupling between neighboring magnetic moments is weak. These magnetic moments tend to align with an external magnetic field, but the magnitude of the alignment decreases at higher temperatures due to random thermal agitation effects. Materially the adjacent magnetic moments are unequal resulting in a net magnetic moment.
- Ferromagnetic materials have pure magnetic moment at the atomic level, but unlike paramagnetic materials there is strong coupling between neighboring magnetic moments. This strong coupling causes a spontaneous alignment of magnetic moments at the macroscopic level, in regions called magnetic fields. The magnetic fields are further aligned under the influence of an external field. They are classified into soft and hard ferromagnetic materials depending on the value of the coherent field (H_c).
- Finally, the antiferromagnetic materials and ferromagnetic materials have neighboring atomic moments oriented antiparallel. In antiferromagnetic materials the adjacent magnetic moments are equal, so that there is no net magnetic moment. In ferromagnetic materials the neighboring magnetic moments are unequal so that there is a net magnetic moment.

3.2. Demagnetization Field

When a sable is magnetized, a field is developed which opposes the magnetizing field. This field is called the demagnetization field and plays a role in the whole process of magnetization.

Let us consider a uniformly magnetized sample of volume V and area S. The magnetization M creates surface poles. These in turn create a demagnetization field H_d within the sample. The demagnetization field H_d is proportional to the magnetization M but in the opposite direction. For example, along the x-axis we have:

$$H_{dx} = -H_d M_x \tag{1}$$

Where H_{dx} and M_x are the x-components of the demagnetization and magnetization fields respectively and N_x is the demagnetization factor along the x-axis. If an external field H_a is applied to the sample, then the field inside the sample Hin will be equal to the vector sum of H_a and H_d:

$$H_{in} = H_a + H_d \tag{2}$$

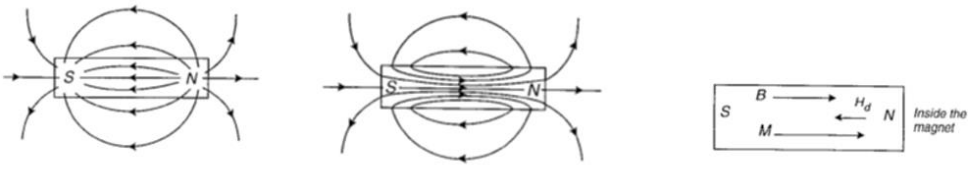

(a) (b) (c)

 doi:10.20944/preprints202312.1678.v1

Figure 10. Permanent magnet field distribution: (**a**) Field H; (**b**) Field B; (c) Field B, H, M within the magnet.

A sample with an isotropic distribution of specific orientation axes (magneto crystalline anisotropy) is considered. It is initially demagnetized with its domains isotopically oriented as shown in point "O" of Figure 11. Applying a H field and as H increases from zero along the positive semi-axis (weak field), the magnetic domains which are aligned with the field grow in size and the oppositely oriented magnetic domains decrease in size due to the movement of the magnetic domain walls. As H increases further (intermediate field) the magnetic moments in the remaining non-oriented magnetic sectors rotate or flip in orientations along specific axes that are in the direction of the H field. For high values of H the magnetic moments along specific axes in magnetic fields not aligned with the H field rotate off these axes and align with H.

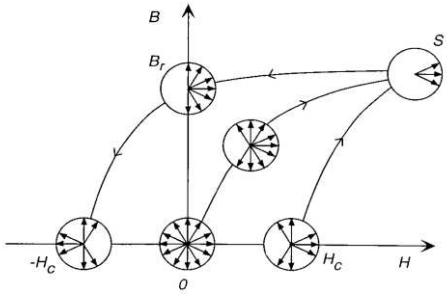

Figure 11. Distribution of magnetic field orientation at various points along the hysteresis loop.

3.3. Hard Magnetic Material Characteristics

Hard magnetic materials are characterized by low permeability and high coherent field value. The latter property makes them difficult to magnetize and demagnetize. Permanent magnets are used as field sources in a wide range of electromechanical devices. One of them concerned the choice of Fe-Co-V alloy instead of silicon steel. The magnetic properties of silicon steel, which is a widely chosen soft magnetic material in motors, deteriorate severely under high pressure, which leads to a reduction in motor performance. In contrast, by choosing this alloy, better torque density, less core loss and better electric motor operation performance were found [61].

The properties of primary importance in the selection of a magnetic material are those that determine the magnitude and stability of the field they can provide. These include the coherent field value H_c, the saturation magnetization value M, the residual magnetization Br, as well as the shape of the hysteresis loop in the second quadrant. This part of the hysteresis loop is called the demagnetization characteristic, Figure 12a.

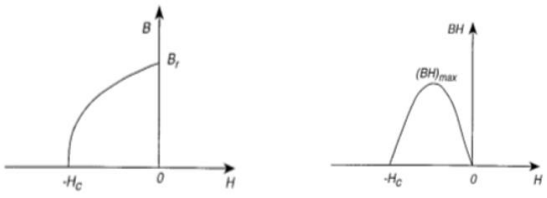

(**a**) (**b**)

Figure 12. B-H second-quadrant curve: (**a**) demagnetization curve; (**b**) B-H function of H.

The points B, H in the demagnetization characteristics define an energy product B-H which takes a maximum value max in the interval $-H_c < H < 0$ as shown in Figure 12b. When a permanent magnet is used as a field source it is polarized at a functional point (Bm, Hm) of its demagnetization characteristic. The operating point depends on the circuit in which it is used. It can be determined from the load line of the circuit. This intersects the demagnetization characteristic at the point (Bm,

 doi:10.20944/preprints202312.1678.v1

Hm) as shown in Figure 13. It is desirable to polarize the magnet at the point of maximum energy (B-H) max. This will result in minimizing the volume of the magnet and reducing its cost.

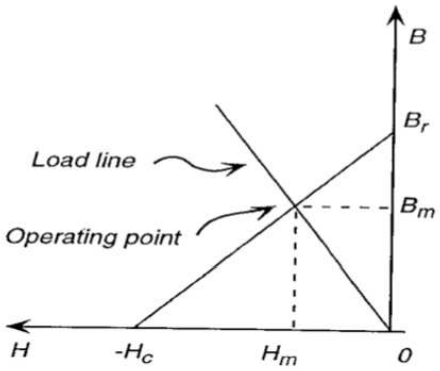

Figure 13. Demagnetization characteristics and load time.

An important consideration in permanent magnet machines concerns avoidance of permanent demagnetization effects of the magnets in cases of faults, as under such conditions the currents can take values several times greater than those of nominal operation. An approximate analysis of the short circuit current variations of the machine, can be performed by using analytical formulae based on sub-transient and transient reactance values, according to the classical two axes transformation method. In general, this method also enables the analysis of machines with damping windings at the poles. The mathematical expression concerning short circuit components time variations are as follows:

$$i_d(t) = -\omega\lambda_{Mag}\left[\frac{1}{X_d} + \left(\frac{1}{X'_d} - \frac{1}{X_d}\right)\cdot e^{-\frac{t}{T'_d}} + \left(\frac{1}{X''_d} - \frac{1}{X'_d}\right)\cdot e^{-\frac{t}{T''_d}}\right] + \frac{\omega\lambda_{Mag}}{X''_d} e^{-a\cdot t}\cos(\omega t) \quad (3)$$

$$i_q(t) = \frac{\omega\lambda_{Mag}}{X''_q} e^{-a\cdot t}\sin(\omega t) \quad (4)$$

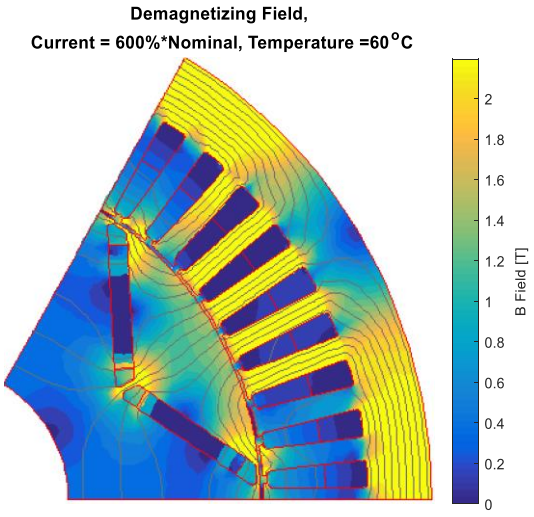

Figure 14. PMSM under short-circuit conditions illustrating one pole part configuration and the magnetic field distribution of an internal permanent magnet V-type machine with inclusion of demagnetization effects at 60°C under short circuit conditions involving stator current density 600% of nominal value.

 doi:10.20944/preprints202312.1678.v1

Figure 14a illustrates the demagnetization effects in the permanent magnets of an internal permanent magnet V-type machine computed by finite element analysis, the geometry if which is shown in Figure 14b.

Permanent magnet motors are now well established in the ever-growing electric car industry. The presence of strong rare earths of Neodymium in these motors is vital for increasing power density [62]. The absence of copper from the rotor offers an advantage for achieving high efficiency, as in the case of modern magnetoresistance motors (SRM), while the presence of magnets improves the power factor and increases the maximum torque capacity [63]. Meanwhile, concerns related to the magnetization level of permanent magnets appear [64]. The main disadvantage of this kind of motors is the difficulty of field attenuation, even at relatively low speeds [65]. The characteristics of the machine are derived from the preliminary design and based on the observe of the high saturation in the rotor and stator. In general, the demagnetization calculation methods are applied on top of some already optimized geometry and help to study the cost, in terms of the type and grade of magnet that the final geometry can use [66–68].

3.4. Thermal Modeling of Permanent Magnets

The dependence of magnetization on temperature is non-linear but approximate models exist [69]. The most common approach is to describe the temperature function with a linear model. This is illustrated in Figure 17 where linearity is established for a local temperature interval, Ti - Ti-1. In this technique it can be assumed that the residual magnetization at the macroscopic level can be approximately correlated with the spontaneous magnetization at the microscopic level.

Magnetization is modelled by a linear function of temperature which decreases with increasing temperature T [70]. Similarly, the residual magnetic induction B_r is modelled by a linear function [71]. It is usually expressed as a percentage per degree Celsius as mentioned above (%/oz) and is given by Equation 5.

$$B_r(\mathrm{T}) = B_r(T_0)(1+\mathrm{a}(\mathrm{T}-T_0)) \tag{5}$$

The above equations express an interval of linearity at a temperature T associated with a reference temperature T_0, which is usually 20 °C. Since the slope of the linear function changes for different temperature intervals, the interval Ti - Ti-1 must be redefined. An analogous model is used to describe the coherent field as a function of temperature.

$$H_{c,i}\ (\mathrm{T}) = H_{c,i}(T_0)(1+\mathrm{b}(\mathrm{T}-T_0)) \tag{6}$$

The parameters of the slope of the linear function in the two models are respectively a, b. Since the IEC standard uses the same symbol a for both models, it is necessary to make the following distinction for two models, a(B_r) and a(H_c) [72].

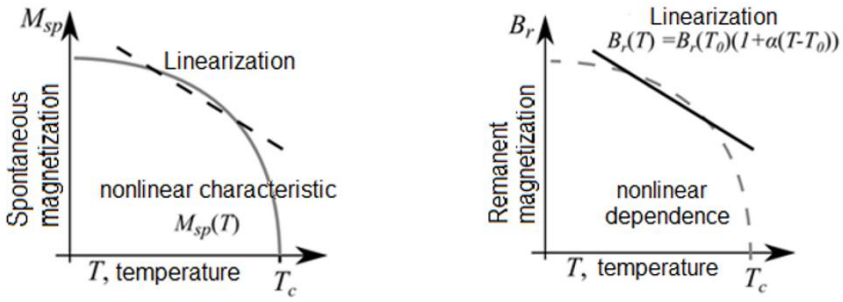

(**a**) (**b**)

Figure 15. Non-linear relationship between: (a) spontaneous magnetization; (b) magnetic induction with temperature.

 doi:10.20944/preprints202312.1678.v1

As the gradient is different T_i - T_i-1 temperature intervals a non-linear model would be more appropriate than the linear one. Such an alternative model has been proposed with second-order polynomials [73] for the residual magnetic induction and coherent field.

$$B_r(\mathrm{T}) = B_r(T_0)(1+a_1(T-T_o) + a_2(T-T_o)^2) \quad (7)$$

$$H_{c,i}\ (\mathrm{T}) = H_{c,i}\ (T_0)(1+b_1(T-T_o) + b_2(T-T_o)^2) \quad (8)$$

Models of permanent magnets are not based on demagnetizing force and residual magnetic induction alone and are not complete without modeling magnetic permeability. A model for the recoil permeability can be developed which takes temperature into account. This can be achieved by a similar linear model originally developed for soft ferromagnetic materials.

$$\mu(\mathrm{T}) = \mu(T_0)(1+a\mu(T_0)\ (T-T_o) \quad (9)$$

The above thermal model of residual magnetization, demagnetizing force and permeability is based on the change of the main parameters. The model can be made more complex if a sigmoid function is used, such as for example the tanh function. To model the B-H curve, the following relation can be used:

$$B_i(\mathrm{H,\ T}) = \mathrm{P(T)}\left(b_0 tanh\frac{H+\mathrm{Q(T)}H_{c,i}(T_0}{Q(T)h_0}\right) + b_1 tanh\left(\frac{H+\mathrm{Q(T)}H_{c,i}(T_0}{Q(T)h_1}\right) \quad (10)$$

Where the fuction P(T) represents the vertical part of the loop associated with the residual magnetization and the function Q(T) the horizontal part of the loop associated with the demagnetizing force.

The ability to impose proper magnetization on magnets to restore full magnetization is a complex problem that requires very stringent conditions to which the magnet must be subjected to make this possible. First, for the study of magnets, a detailed determination of the B-H magnet curve in the second quadrant must be made. For this purpose, according to publication [74], the exponential model for calculating the B-H curve is mentioned. According to the above publication, the function describing the curve consists of two terms, linear and exponential. In order to obtain its correct fitting, it is necessary to determine the values of two constants [75]. The formula of the function and the method of calculating the constants are given below:

$$\mathrm{B(H)} = \mathrm{B_r} + \mu_0\mu_\mathrm{r}\cdot\mathrm{H} - \mathrm{E}\cdot\mathrm{e}^{\mathrm{K_1(K_2+H)}} \quad (11)$$

Where:

- E indicates the units of measurement of the exponential term (1 T or 1 kGauss)
- μ_r denotes the relative magnetic permeability
- $\mathrm{B_r}$ is given by the manufacturer and indicates the residual magnetization.
- K_1 indicates the acidity of the knee; indicative value is -4-10-5m/A for neodymium NdFeB magnets of classical grade (regular grade magnet).
- $\mathrm{K_2}$ is calculated from the equation:

$$\mathrm{K_2} = \frac{\ln\left[\left(\mathrm{B_r} + (\mu_\mathrm{r}-1)\cdot\mu_0\cdot\ {}_\mathrm{j}\mathrm{H_c}\right)\cdot\frac{1}{\mathrm{E}}\right]}{\mathrm{K_1}} - {}_\mathrm{j}\mathrm{H_c} \quad (12)$$

Permanent magnet losses cause an increase in magnet temperature and can lead to a decrease in demagnetization resistance. In order to avoid the negative effects of bifurcations, the above V-shaped MM motor geometry, shown in Figure 14, was considered, which includes an internal MM configuration. Proper evaluation of the demagnetization risk requires combining the permanent magnet loss model with a thermal analysis.

The rotor of the machine comprises permanent magnets of ND50H grade. The calculated magnetic field distribution under short circuit illustrating magnet regions with important demagnetization risks is shown in Figure 14 The demagnetization evaluation is highly dependent on the model used for the B-H curve behavior. Figure 16 shows the percentage of PM demagnetization evaluated by different models implemented. This figure illustrates that at higher temperatures the

 doi:10.20944/preprints202312.1678.v1

simpler models for demagnetization evaluation may lead to important overestimation of the magnet demagnetized percentage.

The study demonstrates that the proposed methodology for the evaluation of permanent magnet bifurcation losses combined with the modeling procedure adopted for the demagnetization consideration can provide great services in the proper determination of the demagnetization risks of MM and the efficient use of the material in the design of electrical machines.

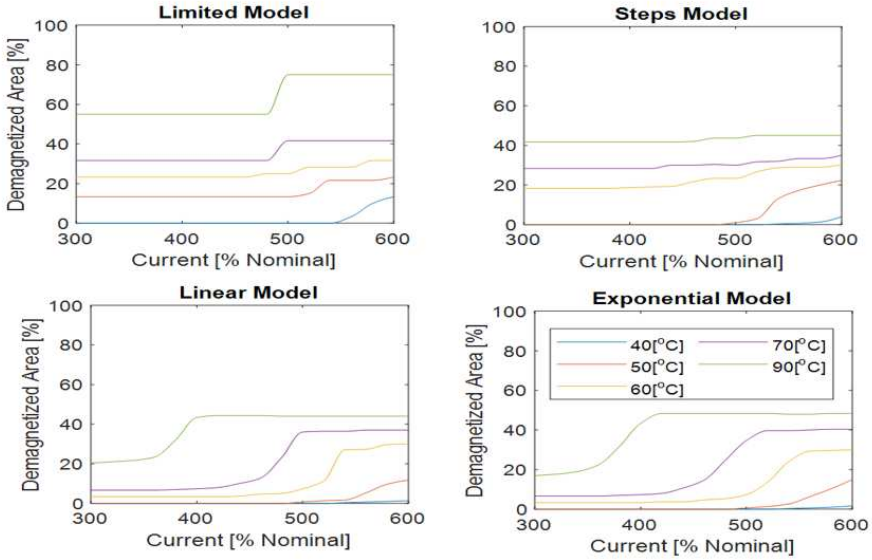

Figure 16. Percentage of the demagnetized area with respect to stator current under different temperatures for ND50H magnet grades.

3.5. Demagnetization Modeling of Permanent Magnets

Permanent magnet motors currently have been established as a favored option in the ever-growing electric automotive industry. In the presence of strong rare earth neodymium material enables substantial increase in power density. In addition, the absence of copper from the rotor offers advantages of reduced maintenance and increased efficiency; on the other hand, in the case of modern reluctance motors (SRM), the presence of magnets improves the power factor and offers the potential for higher torque. A key area of extensive study concerns the level of magnetization of permanent magnets at specific temperatures [76,77].

The following investigation shows in the demagnetization results under three phase short-circuits conditions, in radial flow permanent magnet motors favored in electric mobility applications. The optimization of the geometry was based on the combination of high torque at low speeds and satisfactory performance under field attenuation conditions [78]. Based on the geometry of the motor, three different types of magnets were used in order to draw conclusions about the motor operation in each case. In the motor with ND52 (Figure 17) type there is a strong sensibility to demagnetization even when the stator current is quite low. It is therefore considered quite important to characterize and diagnose demagnetization at an early stage. With the 2D finite element method (FEM) and PMSM motor current examination, which is based on the fast Fourier transform (FFT), harmonics indeed lead to safe conclusions in case of fault as they are characterized as fault indicators for detecting demagnetization. Therefore, the effect of increasing the current is expected to reduce the strength of the machine [79].

 doi:10.20944/preprints202312.1678.v1

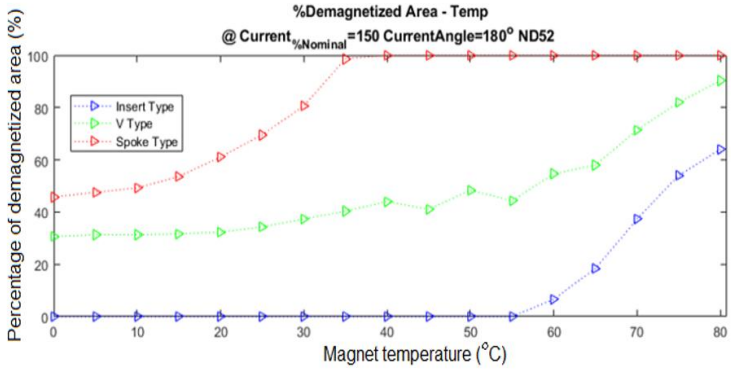

Figure 17. Demagnetized magnet area variation with temperature for a current 1.5 times the rated value at an angle of 180 degrees with reference to the d-axis, in case of ND52 type magnets.

The motors with ND50H magnets were also tested for its demagnetization behavior when the current is 7 times the nominal current as shown in Figure 18. In this case the improvement compared to the previous machine with ND52 magnets is very large.

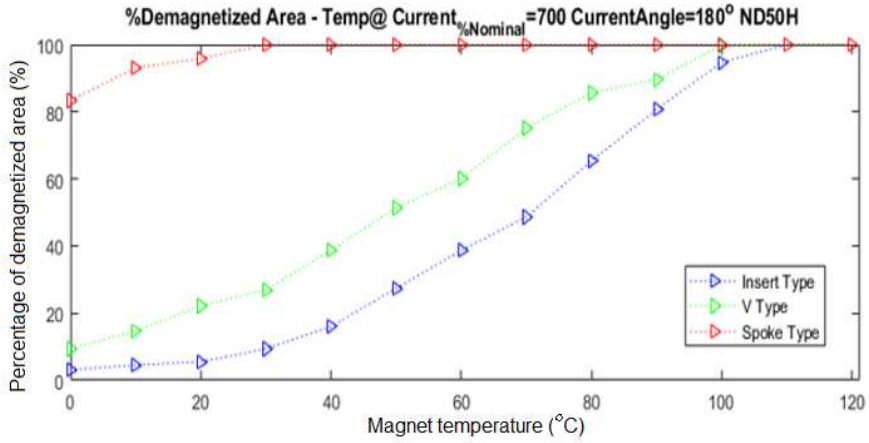

Figure 18. Demagnetized magnet area variation with temperature for a current 7 times the rated value at an angle of 180 degrees with reference to the d-axis, in case of ND50H type magnets.

ND42UH type magnets were then placed in the machine. Magnets of this type have a higher jHc value and are therefore more difficult to demagnetize than ND50H magnets and to that respect even more difficult when related to the original simulation of the machine with ND52 magnets. In order to keep the torque performance of the machine the same, the length of the machine has to be increased, since the Br value of the magnets is reduced [80]. The demagnetization behavior of this machine with ND42UH magnets, as shown in the diagrams below, is much more robust than the previous two machines. This is evident as it shows a strong resistance to demagnetization, i.e., almost zero demagnetization, up to T: 120-180°C and then it demagnetizes abruptly and rapidly.

Preprints.org (www.preprints.org) | NOT PEER-REVIEWED | Posted: 22 December 2023 doi:10.20944/preprints202312.1678.v1

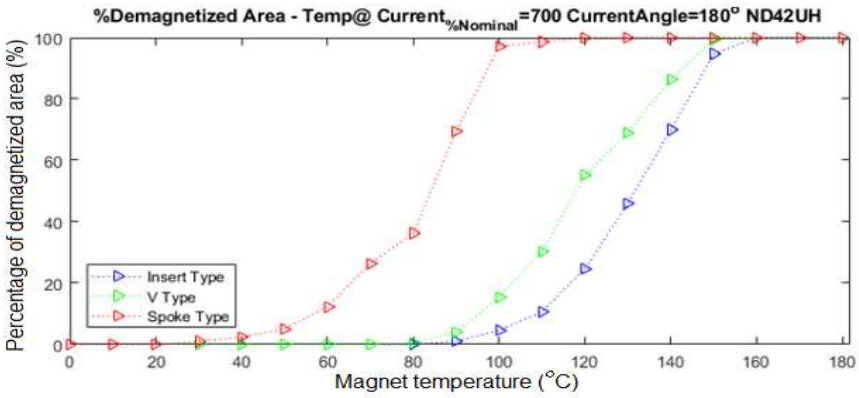

Figure 19. Demagnetized magnet area variation with temperature for current 7 times the rated value at an angle of 180 degrees with reference to the d-axis, in case of ND50H type magnets.

Based on the previous analysis, it is indicated that the method, which was implemented and used, enables easy and fast representation of demagnetization of any configuration of internal permanent magnets as well as any kind of winding and stator geometry. In addition, the power density of the machine increases when the magnets used have higher residual magnetization [81]. This becomes apparent since when the type of magnets is changed, appears a need to vary the active length of the machine in order to maintain the performance at the same torque level. In this way, the power density of the machine is indirectly altered. The demagnetization varies strongly with temperature which can be assessed by the importance of the respective temperature coefficients of the coercive force.

The angle of the stator currents, play a less important but not negligible role in demagnetization of the magnets, as the maximum demagnetization does not occur in all magnets when the excitation field is oriented along 180^0 angle. The geometry of the rotor near the magnets and the local core saturation enables a more uniform distribution of the demagnetization. Finally, the design of appropriate flux barriers next to the magnet borders is necessary to increase the magnet withstand to demagnetization effects by reducing the flux density developed near the magnet endings [82,83].

The final configuration proposed includes two different neodymium magnet grades, that is 42UH and 50H, respectively, while the motor produces higher torque density compared to the motor involving a single magnet grade (ND42UH). In addition, it offers reduced torque ripple and THD while it exhibits greater withstand to demagnetization and lower manufacturing costs. The determination of the appropriate geometry has been obtained by applying the robustness evaluation algorithm in conjunction with the torque calculation algorithm.

3.6. Demagnetization Consideration Methodology

The proposed demagnetization calculation models assume that the demagnetization field is only the component of the field that has a direction parallel to the soft axis of magnetization of the permanent magnet. According to them, during finite element formalism, it is relatively simple, to integrate the respective model into the overall computational scheme.

The stepwise model is an intermediate solution to the restrictive and linear models. It essentially places the demagnetization curve on predefined linear lines. The number of these curves can be relatively small in order to reduce the running time of the algorithm. However, the accuracy is limited compared to the linear model which essentially allows for the generation of demagnetization lines without involving the restriction of the discrete distance between them, which is the case in the step model [84].

Furthermore, the specific methodology developed is based on the stepwise representation of simpler demagnetization models into more accurate and time-consuming models, depending on the results obtained in terms of demagnetized subregions. In particular, successive considerations of the behavior of the B-H curve are adopted: in a first step, the constrained model is explored as this model refers to the recoil curve as a single line passing through the nominal recoil point and to the knee as

 doi:10.20944/preprints202312.1678.v1

a constrained function that sets the recoil line to zero recoil, and then the step model is applied, using a predefined number of recoil lines and the same knee definition line as before; in a next step, the linear model is introduced, including two types of lines for the if Finally, the exponential model is applied, using two exponential curves with defined knee parameters, which form the recoil curve and the behavior of the B-H knee. These models obtained for the ND50H magnet class at 20°C are shown in Figure 20.

Consequently, the first FEA analysis is performed with the standard representation of the permanent magnet and then according to the local magnetization results a recursive algorithm introduces the new recoil curves consecutively, if needed.

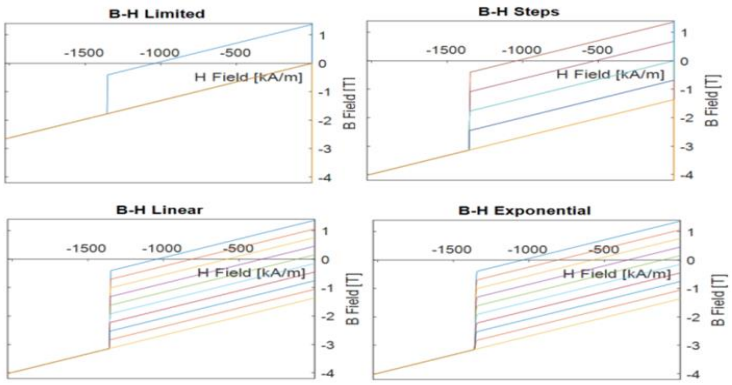

Figure 20. B-H curves and recoil models derived for ND50H magnet grade at 20°C.

4. Combined Permanent Magnet and Lamination Loss Modelling

Surface-mounted permanent magnets present design advantages due to the creation of a strong magnetic field in the gap of electric motors but are sensitive to the development of eddy currents [85]. These are generated by harmonic phenomena due to stator slotting during rotor rotation and switching frequency effects involved in pulse-width modulation techniques applied in inverter supply [86]. In the recent literature, numerous techniques for loss estimation in permanent magnets have been developed [87], indicating the dominance of losses due to eddy currents over hysteresis losses in most practical electric motor applications [88].

In order to reduce the losses due to eddy currents, the magnet segmentation method can be applied. However, even in segmented magnets, the harmonics generated by the supply usually involve penetration depths less than the size of the segments [89]. To that respect, there is a need to account for the third dimension in the magnet end regions when modeling the generated eddy currents in order to accurately calculate the losses they generate while using a Two-Dimensional Finite Element Analysis [90].

A methodology based on the 3D Fourier Transform (3D FFT) method has already been proposed in the literature [91]. Moreover, a technique has been introduced, enabling evaluation of eddy current losses in permanent magnets, by using a Two-Dimensional Finite Element Modeling (2D FEA) combined with differential resistance concept in the magnet's end regions.

Another methodology introduces lumped parameter impedances by developing an already well-established technique for considering the end region of the rotor damper windings. The skin effect of the magnet is taken into account through appropriate techniques involving mutual inductances in lumped parameter models. In addition, a C-core type magnetic circuit has been modeled through both three-dimensional and two-dimensional finite element analysis and validated by measurements. In addition, a methodology for separating the core and permanent magnet losses, through consecutive experiments has been presented and implemented [92].

4.1. Experimental Setup

In order to properly model the losses in permanent magnets, a specific simple magnetic circuit was constructed. This magnetic circuit consists of two U-shaped sections with wound coils and a core

 doi:10.20944/preprints202312.1678.v1

made of soft magnetic material, separated by two neodymium allow magnets. Two copper coils are wound around the position where the magnets are placed. These windings are used for excitation purposes and for detecting the included voltage, as shown in the diagram below. In the first step, the losses in the core were measured without the presence of the permanent magnet. In the second step, the magnets were placed in the magnetic circuit, and the total losses were measured at various frequencies. This two-step process allows for the precise determination of eddy current losses in the permanent magnets.

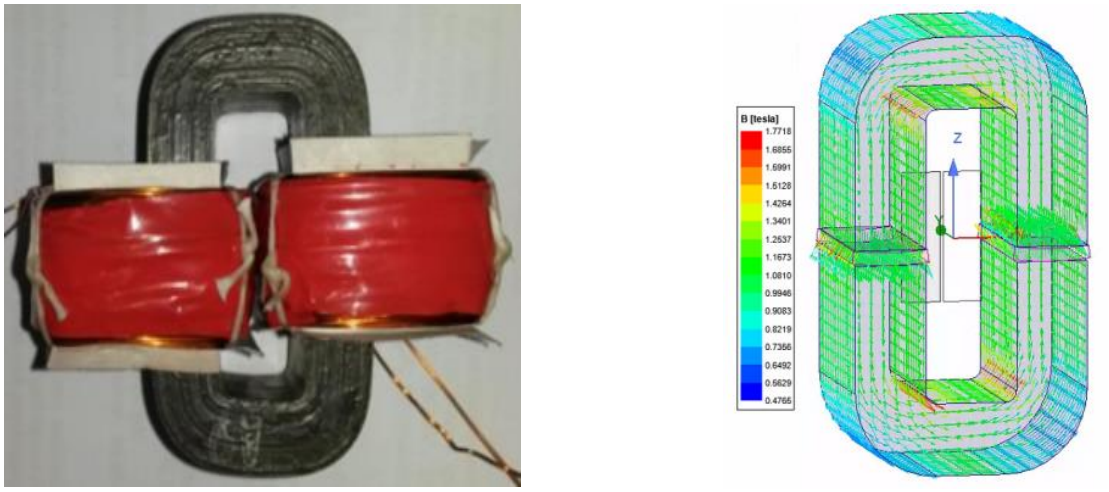

(**a**) (b)

Figure 21. Magnetic circuit considered for losses validation: (a) Experimental magnetic circuit configuration. (b) Flux density distribution for AC current of 0.06A at 10kHz.

4.2. Core Loss in C-Core Magnetic Circuit

The core loss model is based on the Bertotti's separation of losses technique [93], which is expressed by Equation 13.

$$P_{Core} = K_H B^2 f + K_C B^2 f^2 + K_E B^{1.5} f^{1.5} \quad (13)$$

Where:

- K_H=1.05·10^{-2}[7.W/(kgT^{2}Hz)] represents the hysteresis loss coefficient.
- Kc = 7.91·10^{-5}[7.W/(kgT^{2}Hz^2)] represents the eddy current loss coefficient.
- K_E = 3.16·10^4[7.W/(kgT$^{1.5}$Hz$^{1.5}$)] represents the excess loss coefficient.

The excitation coil of the magnetic circuit consists of 24 turns and the magnets are absent during the experiment. The coefficient K_H, Kc and K_E were derived from measuring losses under various loading conditions. In the diagram below, the measured losses are presented for different frequencies and maximum flux density values (B_{max}), along with the corresponding adjusted surface area obtained [94]. A similar technique is followed to calculate the iron losses to induction motors with PWM supply from an inverter involving good precision in iron losses evaluation [95].

 doi:10.20944/preprints202312.1678.v1

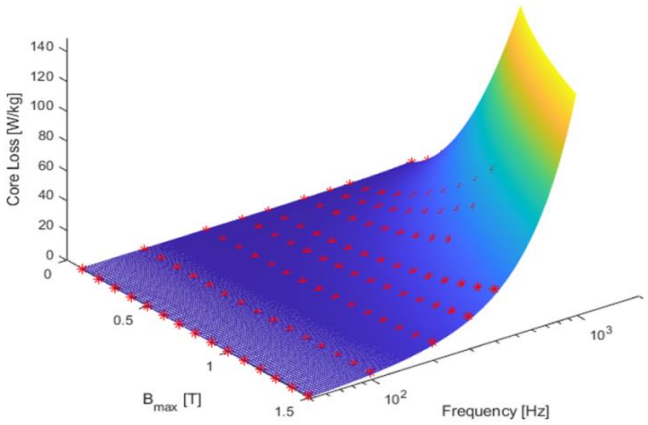

Figure 22. Core loss and the fitted surface of the core loss model with variations in frequency and flux density.

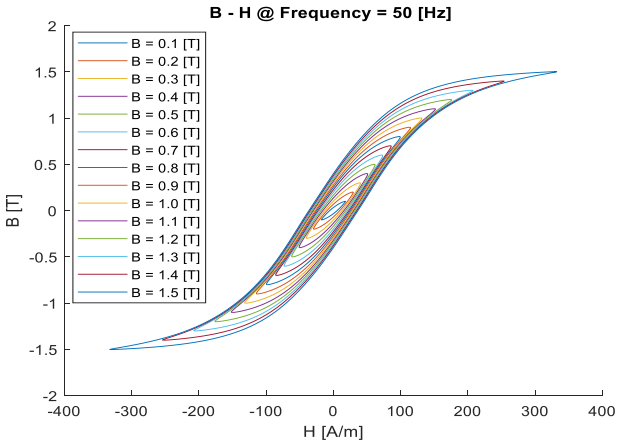

Figure 23. Experimental assessment of the hysteresis loops of soft magnetic material. Family of curves at a specific frequency of 50Hz for different maximum magnetic field intensity variation.

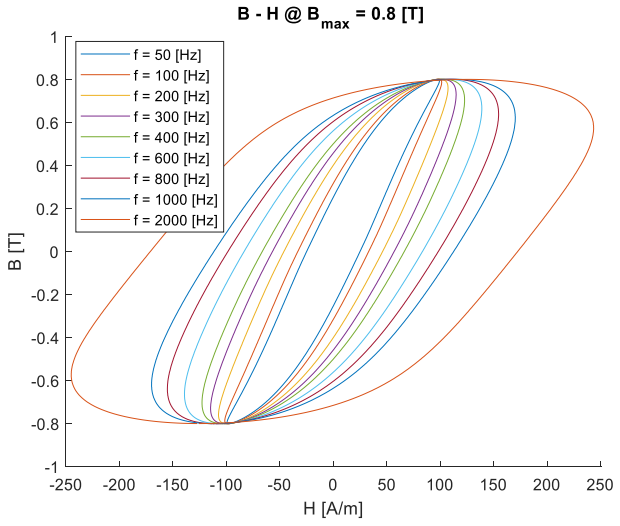

Figure 24. Experimental assessment of the hysteresis loops of soft magnetic material. Family of curves at a specific magnetic flux density amplitude of 0.8T as a function of excitation frequency.

 doi:10.20944/preprints202312.1678.v1

4.3. Magnet Losses

In order to properly evaluate the losses in the permanent magnets in a magnetic circuit as the one shown in Figure 21, it is needed to separate the core losses from the total losses. Moreover, the choice of stator design and the supply by modern inverters with high switching frequency introduce harmonics that can contribute to significant losses in the magnets, causing the rotor to heat up [96]. To that respect, the aim to exploit the advantages of permanent magnets in modern machines have prompted several researchers to increase the frequency of electromechanical energy conversion by examining in detail the losses of the magnets [97,98].

The FEA modelling process requires usually an examination of three-dimensional configurations due to the geometries of the applied permanent magnets and the paths of the developing eddy currents. Additionally, the nonlinear characteristics of the cores necessitates a step-by-step time representation, resulting in a demanding framework concerning memory and execution time constraints [99].

In order to develop efficient models for estimating losses due to switching frequency in the runner of surface-mounted permanent magnets, mixed numerical techniques coupling field and circuit equations have been proposed for cases involving pulsed width modulation (PWM) power supplies [100,101]. Such models are based on a Two-Dimensional Finite Element Analysis (2D FEA) combined with circuit equations in border areas of the permanent magnets. The analysis takes into account the extreme end effect phenomena associated with the switching frequency, which are primarily responsible for the majority of eddy current losses in the magnets [102]. It is worth noting at this point that a significant part of the losses relates to the existence and occurrence of harmonics inside the machine. The harmonic content in the PMSM flow due to stator grooving was determined in [103]. The currents in a solid rotor of a PMSM due to stator indentation were calculated in [104], taking into account magnetic saturation. It was shown that the harmonics of the teeth decrease with saturation and, consequently, the respective losses were lower.

The model's accuracy is validated through experimental measurements in magnetic circuits. The comparison between the experimental losses and the losses predicted by the model was made by applying a basic loss segregation analysis and highlighted the dominance of losses due to eddy currents in permanent magnets associated with the switching frequency [105]. In case that the air gap field contains only synchronized spatial harmonics, the magnetic bisection losses can be neglected. Similarly, in real situations, the magnetic flux density in the air gap has a spatio-temporal variation: therefore, non-synchronized spatial harmonics are generated. Therefore, significant losses are caused by eddy currents in the rotor [106].

Particular 2D Finite Element methodologies combining end zone circuits, in order to take into account the currents flowing in permanent magnets end zones, have been created by using both time discretization techniques based on harmonic analysis through complex variables, and FDTD including time-stepping techniques [107].

The magnetic circuit shown in Figure 21 supplied by sinusoidal waveform current at 1kHz up to 20kHz, corresponding to switching frequency of SPWM supply, presented comparable losses in laminated iron and permanent magnet parts, illustrating a dominance of the latter in higher frequency ranges. Moreover, the simulated results obtained by the 2D coupled method were in good agreement with the those of the 3D FEA model and the respective experimental ones [108].

These results demonstrated that such modelling procedures are promising for efficient simulation of magnet eddy current losses, which are generated by the intermittent frequency of the carrier signal used in pulse-width modulation in inverter-driven surface permanent magnet machines [109]. It may be noted that such techniques are necessary as the standard two-dimensional finite element analysis without coupling with the circuit equations results in significant overestimation of the eddy current losses in the magnets.

In [110] by applying such a method, a parametric design study has been performed, enabling significant reduction of the computation time and allowing optimization of key machine parameters.

In the above mentioned analyses the governing equation is the diffusion equation expressed in Cartesian two-dimensional formulation in terms of the magnetic vector potential, while at the same

 doi:10.20944/preprints202312.1678.v1

time the gradient of the electric scalar potential enables consideration of the end region effects of permanent magnets [111]. A similar approximate analysis has been developed, reflecting the calculation of the magnetic field in two-dimensional problems in which a region with a space-varying magnetic parameter is defined extending the Maxwell-Fourier method for the simulation of surface-mounted high-speed cylindrical permanent magnet machines [112].

4.9. Experimental Validation in a LinearMotor Prototype

Permanent magnet motors are a preferred choice in electrification applications in particular in respective initiatives in transport, due to their relative advantages of increased efficiency and the absence of rotor excitation requirements. This characteristic presents important advantages in high-speed ranges [113]. However, the generation of significant fault currents as well as the subsequent risks of permanent magnet demagnetization and impact on the behavior of the drive system significantly increase concerns related to the appropriate configuration for each class of electromobility application [114], [115].

A wide range of studies and analyses have been developed on losses in the permanent magnets of inverter-fed motors [116]. The studies focus on different types of motors, such as surface mounted PM synchronous motors and IPMSMs, as well as on various types of permanent magnets such as NdFeB and SmCo alloys [117]. High harmonic effects excite the high-speed leakage losses such as eddy current losses in surface-mounted permanent magnets [118,119]. Internal permanent magnet configurations facilitate the reduction of leakage losses but suffer from withstand limitations in high-speed applications due to rotor dynamics [120]. With this in mind, the switching frequency harmonics are responsible for a significant part of the losses in high-speed permanent magnet motors supplied by PWM inverters [121,122].

Coupled field and circuit methodologies facilitate the appropriate optimization of the geometry of permanent magnet motors. Intermittent frequency losses can be appropriately included in terms of the magnetic field and electric circuit coupling equations, thereby separating iron and permanent magnet losses over a range of high frequency conditions [123]. Such a technique offers improved computational efficiency for the prediction of eddy current losses, using a specific two-dimensional finite element analysis (2DFT). Moreover, superposition principle considering frozen local iron permeabilities associated to low frequency effects and incremental permeabilities associated with the switching frequency due to PWM power supply, allows fast calculations compatible with the optimization procedure adopted [124].

The methodology is related to the calculation of the switching frequency losses developed in the iron laminations. Initially, the degree of saturation of the iron parts due to the fundamental supply frequency is considered, and then the dynamic losses dominated by the eddy current losses and the contribution of dynamic excess losses in the iron parts and permanent magnet parts are estimated.

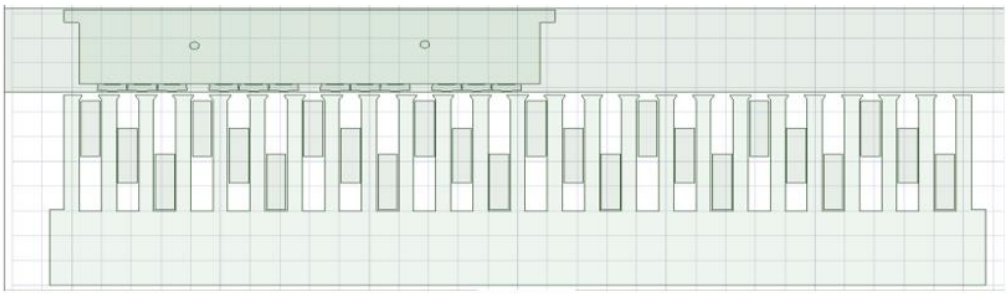

(a)

 doi:10.20944/preprints202312.1678.v1

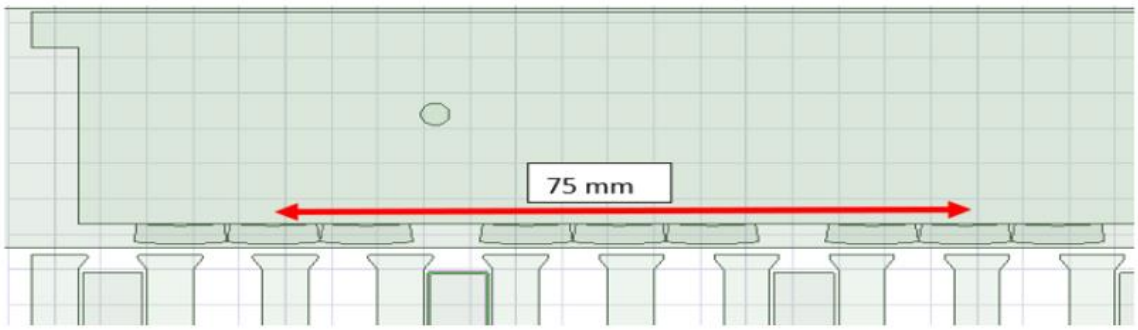

(b)

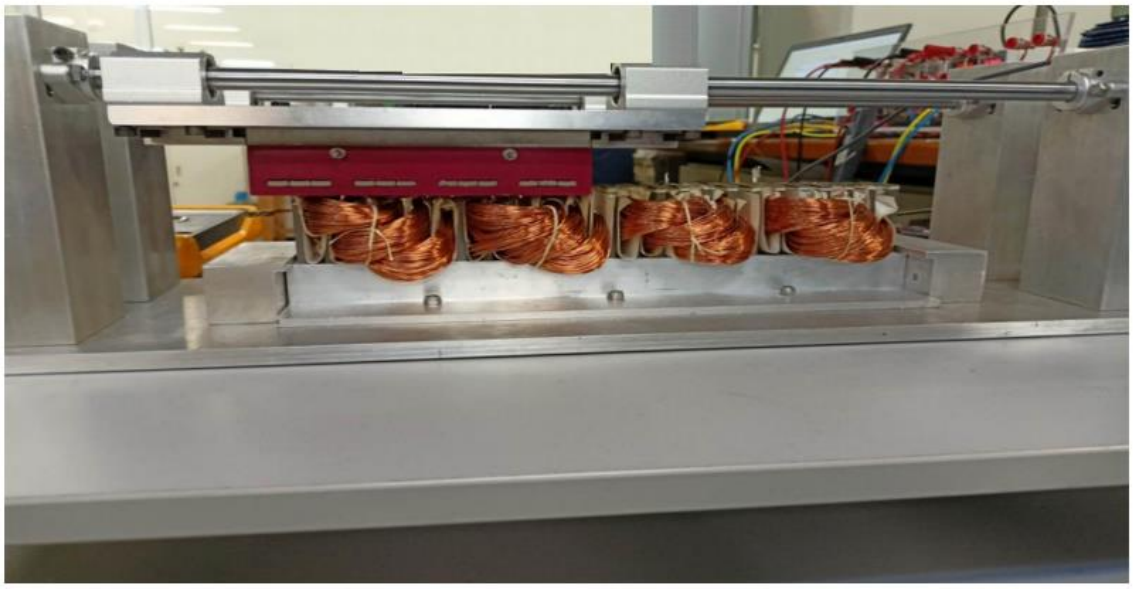

(c)

Figure 25. Prototype magnetic circuit of a linear permanent magnet machine: (**a**) Geometry of the linear machine configuration; (**b**) Distance covered by the rotor in one period of time; (**c**) Manufactured prototype.

Still high harmonics due to slotted geometry and switching supply waveforms, as well as the DC magnetic field bias due to PM flux, greatly affect the iron losses during the operation of a PM motor [125]. The above mentioned modelling techniques have been validated through measurements on a manufactured prototype linear magnetic machine circuit with surface magnets mounted on the rotor, shown in Figure 25c.

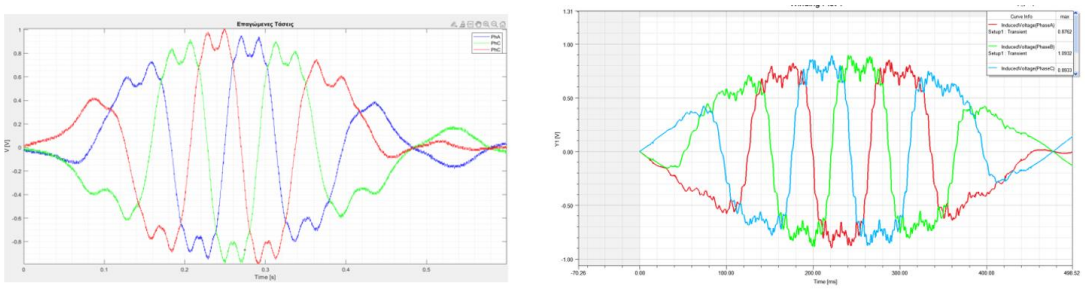

(a) (b)

 doi:10.20944/preprints202312.1678.v1

Figure 26. Comparison of total losses between experimental measurements and those calculated using the proposed methodology: (**a**) Experimental Back-EMF results from induction at the ends of the windings; (**b**) Simulation results Back-EMF from induction at the ends of the windings.

With the implementation of the experimental part, the confirmation of the Back-EMF which is developed at the ends of the windings of the linear machines is achieved. In the machine that a horizontal force was applied to its movable part which caused the its accelerated motion. With the aid of the oscilloscope (shown Figure 26a), the Back-EMF was measured developed in the windings of the three phases due to this movement and the result confirmed the simulation with a fairly good accuracy (shown Figure 26b).

Table 1. Comparison of laboratory measurements with simulation results.

Results	Parameters	Value
Maxwell Simulation	Fundamental amplitude (mV)	962
	THD (%)	25.8
Laboratory Measurements	Fundamental amplitude (mV)	984.3
	THD (%)	19,62
Error	Fundamental amplitude (mV)	2.2%
	THD (%)	23.9%

According to the above curves we observe that both the experimental and the simulated Back-EMF curves converge with each other demonstrating the accuracy of the methodology applied. The divergence of the fundamental amplitude between experimental and simulation is quite satisfactory (2.2%) as it depends on the interaction of the magnetic fields at one-pole pitch, but the same is not the case between the EED distortion coefficients from the harmonics for the two waveforms (23,9 %), as there is a strong dependence on the local tooth-spring geometries that are sensitive to manufacturing defects. This study introduces a specific design methodology for permanent magnet motors for electrification applications. The methodology includes efficiency and power density criteria coupled with criteria for avoiding magnet demagnetization risks in fault conditions, using coupled magnetic field and electric circuit equations, thereby enabling efficient modeling through two-dimensional finite element analysis. In addition, another technique involves the design of a Machine Learning (ML) based demagnetization fault diagnosis method for PMSM motors. The time-frequency domain analysis based on the short-time Fourier transform (STFT) is applied to the process of extracting failure characteristics of PM from the stator phase current signal [126].

In addition, to measure the losses in the stator laminations, the permanent magnet rotor can be easily removed from such a prototype. In a first step the rotor was kept stationary and the stator winding was powered by a sinusoidal AC source, providing 1200At excitation at a frequency of 10kHz (shown Table 2).

Table 2. Measured total losses variation with sinusoidal excitation current in the linear motor prototype for different frequencies in both cases of rotor presence and without rotor.

f=1kHz		f=5kHz		f=10kHz		f=15kHz		f=20kHz	
Excitation (At)	Losses (W)	Excitation (At)	Losses (W)	Excitation (At)	Losses (W)	Excitation (At)	Losses (W)	Excitation (At)	Losses (W)
8	0.1	9	0.1	8	0.2	9	0.3	9	0.5
12	0.2	13	0.2	11	0.3	11	0.4	12	0.8
14	0.3	16	0.4	14	0.5	15	1	15	1.5
18	0.4	19	0.5	17	0.7	18	1.5	19	2.1
20	0.5	22	0.8	21	1.2	22	2.1	23	3.1

 doi:10.20944/preprints202312.1678.v1

24	0.6	25	1	24	1.5	25	2.8	26	4
26	0.7	28	1.2	27	2	29	4	29	5.8
28	0.8	31	1.8	30	2.8	32	4.5	34	6.5

Based on the above results we observe that permanent magnet losses are proactively negligible at low frequencies, while they become very significant in the high frequency regions. Moreover, the good agreement assessed between the measured and simulated losses at all frequencies considered demonstrated the validity of the proposed methodology in this class of problems and its suitability to be applied to surface-mounted high speed permanent magnet motors [127], [128}. This table shows that the losses in the permanent magnets are comparable to those developed in the laminated parts of the stator in all frequencies considered. The techniques introduced achieve adequate modelling of high frequency losses, as validated by measurements on a prototype magnetic circuit, and ensure robustness of the design, which is of major importance in high speed applications.

5. Mixed Numerical Techniques for the Simulation of Permanent Magnet Machines

Permanent magnets (PM) are usually represented in electrical machines by using the finite element method (FEM) combined with other methods in order to calculate parameters and analyze phenomena developed in permanent magnets; such techniques have been extensively applied by researchers to overcome the problems of computational complexity (mainly posed by 3D finite element analysis) and to improve the accuracy of the method. In the followings, representative related work reported in the international literature over the last two decades is presented.

A method that combines 2DFEM results along radial sections of the geometry, called quasi-3D FEM is proposed for the analysis of PM machines in [129]. Relying on the disadvantage of quasi-3D FEM is its inability to conduct finite element analysis when the rotor back iron and permanent magnets have different lengths along the radial direction. Thus, an improved technique was applied combining asymptotic boundary conditions with finite element method to improve the calculation accuracy and computational efficiency [130].

A proposed strategy uses a Response Surface Methodology (RSM) to dynamically reset the objective function according to its optimization objective. Analytical functions are used in order to verify the proposed method is feasible and capable of reducing the computational time. The numerical example of the optimal design of a PM motor shows that the computer program developed based on the proposed algorithm can significantly reduce the FEM simulation times and speed up the optimization while ensuring the accuracy of the dual RSM [131]. Scmidt and Susic [132] and de Assis et al. [133] use the Frozen Permeability Method (FPM), which performs a discrete analysis of fields induced by different excitation sources, in combination with FEM to calculate permanent magnet synchronous motor parameters [134].

A work proposed an accurate tubular permanent magnet linear motor (PMLM) iron loss calculation model combined with finite element method in which the effect of the primary motor structure harmonics on core losses are accurately calculated [135]. Xie et al. use coupling of analytical models, FEM and CFD for electromagnetic and thermal analysis of low-speed PM motors [136]. The simulation and measurement curves showed that high copper loss of the stator winding is observed at the location of the highest temperature rise of the system. The results demonstrate that as the fluid flow rate accelerates, the system temperature rise decreases at an inversely proportional rate. Finally, after a tipping point, the system temperature stabilizes. Similarly, Chen et al. apply such techniques to high-speed train motor applications [137].

In [138], a new transverse flux permanent magnet linear motor (TFPMLM) is constructed, which is called double-sided double excitation; using the Schwarz-Christoffel (SC) mapping method enabled efficient analysis of the magnetic field and motor characteristics. Genetic Algorithms (GA) have been implemented in conjunction with coarse FEM to optimize the magnet positions and their effect on the motor characteristics [139]. The distribution of the aerodynamic field in the air gap of the electrical motor has been equally evaluated and its impact on the thermal analysis as well as the

 doi:10.20944/preprints202312.1678.v1

functionality of the method in comparison to other techniques, has been assessed [140]. In addition, other techniques for optimizing and examining key motor parameters combining multi objective optimization and using Finite Element Analysis (FEA) have been proposed [141,142].

6. Mechanical Analysis of Electrical Machines

6.1. Mechanical Deformation Effects

Recent developments in power electronics favor high speed permanent magnet machines which are widely used in electric drive applications due to their advantages in terms of achieving high power density, efficiency, durability, and low maintenance costs. High-speed motors are generally vulnerable to the development of critical eddy current and core losses, which promote the selection of low thickness and/or high silicon concentration laminations during design [143]. Moreover, a possibility to reduce losses is the design of multi-phase motors. Their advantages are the generation of a field with less space harmonics and therefore better efficiency, with reduced time harmonic content [144] thus decreased torque oscillations at frequencies several times the fundamental frequency and better fault tolerance [145], since in the event of a fault, the phase showing damage can be isolated at the expense of slight degradation of the power generation capability of the machine and small reduction in the starting capability [146]. Also, the multi-phase machines with concentrated windings can increase that torque generating capacity by introducing appropriate higher harmonic current components from the inverter [147].

The power source is realized by using adequate power converters, so driving multi-phase motors is feasible provided that suitable power converters are designed [148]. The need of electric vehicles for high power density (resulting in low weight and volume) has led to the design of suitable inverters where the increase in power density will be realized by using wide band gap semiconductor power devices such as SiC or GaN, mainly due to their capabilities of being very small and capable of operating at high frequencies [149]. Multi-phase power converters have the additional advantages of improving the noise characteristics and that for their configuration power electronics can be used with less rated power than the corresponding three phase converter [150].

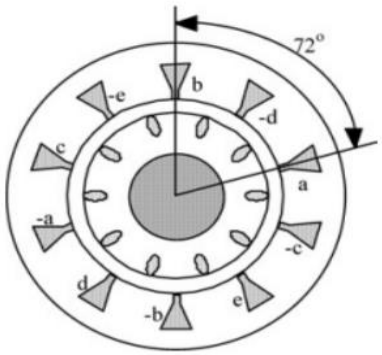

Figure 27. Concentrated winding 5-phase induction machine [146].

 doi:10.20944/preprints202312.1678.v1

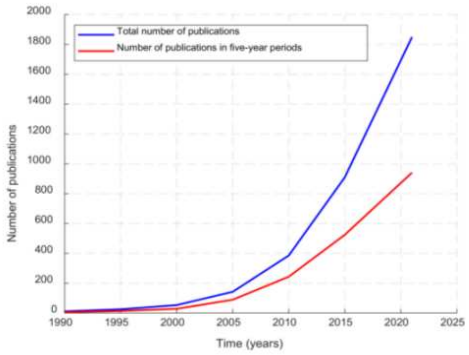

Figure 28. Concentrated winding 5-phase induction machine [151].

In high-speed applications, rotor design involves trade-offs between opposing goals, such as ensuring reduced flux leakage, reduced magnetic laminations losses and lower rotating mass while maintaining increased magnetic drag torque [152]. Another key objective is to achieve a reduction in rotor mass, especially in areas where the flux density shows significant saturation, such as in permanent magnet supports [153]. A special category of modern motors are hysteresis motors where the output torque is produced through the hysteresis effect of magnetic materials and the rotor is made of magnetic material that exhibits hysteresis losses. The results are to develop hysteresis torque which is constant at all speeds but can be used in very small applications due to low efficiency, power factor and torque [154]. The main advantages of its use are its simple structure, its operation at high speeds, resistance to high temperatures, low noise and self-starting ability. Its application is quite limited in some special cases that require high speed such as electric vehicles and high stagnation [155]. The combination of these challenges can lead to unpredictable critical deformations of the rotor surface, resulting in a reduction of the gap length and bringing about changes in inductances along the normal and vertical axes, as well as torque oscillations. A not very common category of machines, but one that has been the subject of much more research and has been developing in recent years, in the category of machines using a magnetic counterpart, the Magnetically Geared Machines (MGMs), involving structures shown in Figure 29. This type of motor is capable of either increasing or decreasing the revolutions per minute in order to respond to different load profiles, as in the case of mechanical gearboxes, but with physical isolation between rotating components [156].

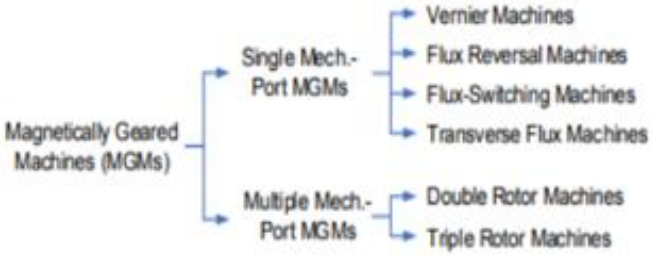

Figure 29. Categories of **c**oncentrated winding 5-phase induction machine [157].

The mechanical stresses and deformations under the influence of centrifugal forces of the runner blades can be analyzed using a 2D triangular mesh. The stress limits of the tested materials can be based on manufacturer's data and compared with the von Mises stress calculation to check whether the laminations can withstand the stress developed by the radial forces [158]. The mass of the rotor and its ability to withstand centrifugal forces at maximum speed conditions can be entered into an objective function of an appropriate evolutionary optimization algorithm to obtain the preliminary geometry for the rotor design. The electromagnetic behavior can then be investigated by the Finite Element Method with a non-linear Discrete Image Solver in the Time Domain from the previously generated mesh. According to sources [159,160] refer to investigations on the effect of stresses on

 doi:10.20944/preprints202312.1678.v1

the relative permeability of iron which have been carried out respectively for the stator side, due to the tight assembly as a way of mounting the stator [161].

In relevant studies, a combined mechanical and electromagnetic analysis has been adopted and specific techniques for the weak coupling of the interdependent phenomena have been proposed. Various types of mechanical eccentricities with respect to rotor positioning can cause severe damage and reduce its ability to rotate at higher speeds. Therefore, advanced finite wavelet techniques have been developed that allow the detection of such eccentricities [162]. A variable magnetic resistance rotor shaft operating under high-speed conditions is studied in the source [163], together with some characteristics related to the machine drive inverter.

6.2. Mechanical Analysis in Electrical Machines

6.2.1. Vernier Machines

The energy losses introduced by the use of a gearbox where a proper interface with the electric motor is required and significant reliability issues [164], due to thermal and mechanical stresses, reduce the lifetime of the motor, thus prompting the exploration of possible alternative applications [165]. Vernier machines are a solution to this problem for low power applications and high torque requirements with direct motor drive, since for given volume, some topologies can produce torque two-three times higher in comparison to a conventional motor. The main reason that this type of electric motor has gained great interest in the last two decades is due to their high torque density, which is made possible by the magnetic gearing effect [166]. The possibility of increased torque production (+40% on average compared to traditional permanent magnet machines) is due to the interaction phenomena of the harmonic content of the rotor magnets with the harmonic content of the of the coils of the groove coils [167].

Some of the applications where Vernier machines are encountered include traction systems [168], linear permanent magnet vernier generators manufactured to harness the energy of sea waves [169], wind turbines [170], rotary vehicle motors [171], axial flow autofocus lenses with ring magnets [172] and linear generators without pistons [173]. The characteristic of the machines is the transmission ratio which is defined as the ratio of the number of pole pairs of the rotor to the number of the stator. The three basic characteristics of a Vernier machine are the rotor design, the flux modulation poles (FMPs) and the winding configuration of the machine.

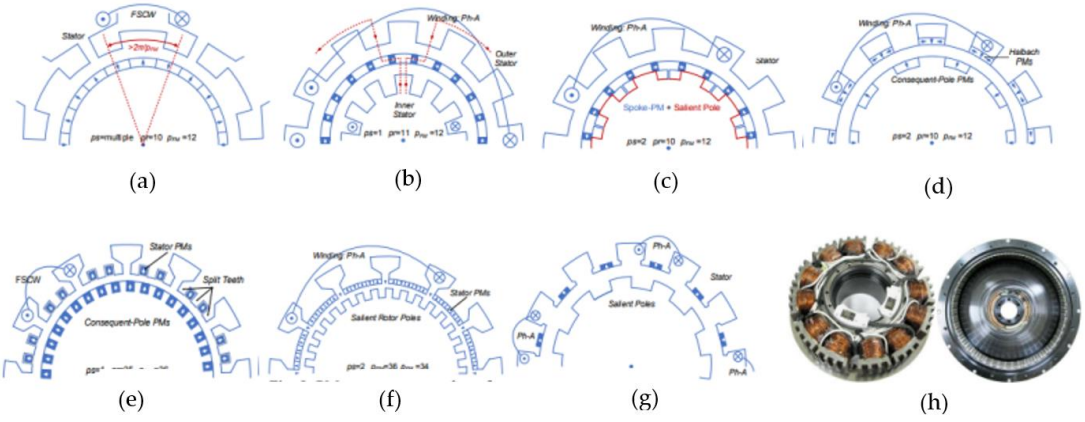

Figure 30. Examples of Vernier machines: (**a**) Non-uniform FMP design; (**b**) Spoke-PM with double stator; (**c**) Alternating flux barrier scheme; (**d**) Stator-PM in slot-opening; (**e**) Stator-PM inserted btwn tooth; (**f**) PM mounted on tooth surface; (g) Stator-PM inserted in teeth; (h) Assy of a modular PMVM [157].

 doi:10.20944/preprints202312.1678.v1

6.2.2. Flux-switching Electrical Motors

As in the case of the Vernier machines discussed above, permanent magnet variable flux machines have been of increasing interest in recent years, due to their numerous advantages such as high flux density due to flux concentration phenomena, good management of the heat generated, and magnets that can be placed in the stator with relative safety in terms of demagnetization and suitability for high-speed applications. An important role is played by the appropriate design of the rotor as an iron body, without the limitations introduced by centrifugal forces in conventional machines [174].

Compared to other machines with magnets in the stator, alternating flow machines have better torque and power density and more sine-wave anti-EMF. Disadvantages include reduced space for windings in the stator grooves due to space occupied by the magnets, the higher cost of using quantity of magnets and manufacturing difficulties due to the particular stator configuration. They also exhibit a high torque ripple due to the structure double-printing structure and high flux density with the occurrence of saturation phenomena in the magnetic circuit [175].

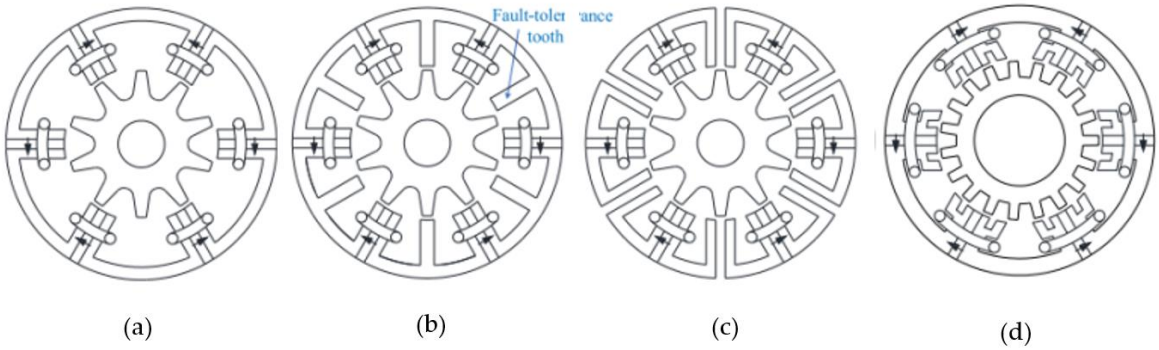

Figure 31. Topologies of variable flow machines: (**a**) C-core; (**b**) E-core; (**c**) Modular stator; (**d**) Multi-tooth [168].

Figure 32 illustrates the operation of the machine as a generator. The operation as a motor is based, like in the Vernier machine case, on the magnetic differential effect, which is the equivalent of a mechanical gear, with the advantage of not having the wear and tear that it suffers but with the disadvantage of increasing the cost. The aim is for a small movement of the rotor to cause a large change in the magnetic flux and a high torque output. H interaction of the magnets multiplies or divides respectively the number of revolutions and the torque between the two rotating parts [176].

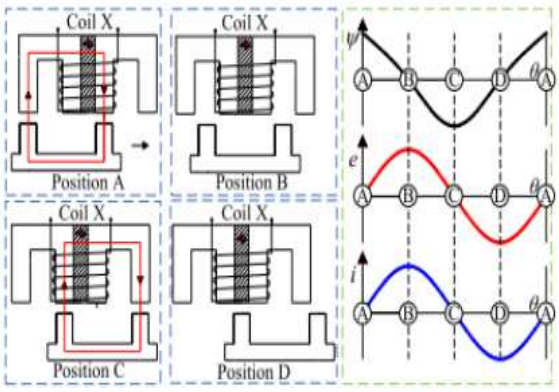

Figure 32. Working principle of variable flow machines [168].

6.2.3. Flux Reversal Electrical Motors

These machines have, like the variable flow machines, magnets in the stator. The difference is that the magnets are located inside the teeth of the stator and, unlike other machines with magnets

 doi:10.20944/preprints202312.1678.v1

in the stator, in this case we have a simpler and sturdier construction with easy placement of the magnets and without reducing the space available for the excitation winding in the slots. The flux, generated by a pair of permanent magnets on a tooth of the FRM, is closed at the stator tooth and along the tooth, respectively, which creates a variable flux connection. [177].

Figure 35 below shows how simple the rotor is and how complex the stator is for this type of machine and, accordingly, their manufacturing process.

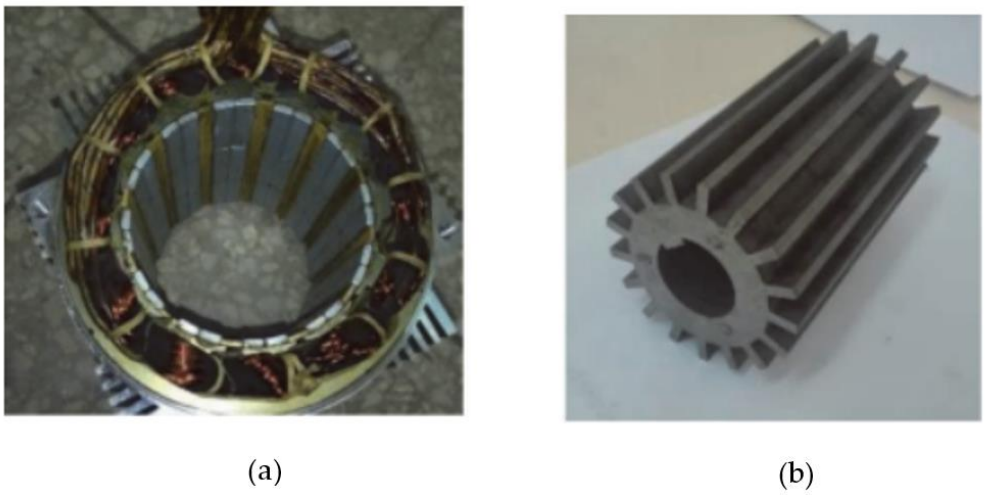

Figure 33. Flux reversal machines: (a) Stator; (b) Rotor [178].

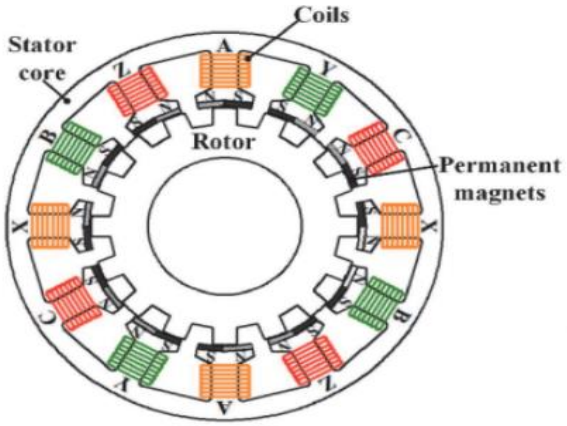

Figure 34. Typical geometry flux reversal electrical motors [178].

6.2.4. Special Electrical Motors

Electrical motors with more than one stator or rotor appear in the literature. These are variations of the main categories studied above and designed for specific applications such as servo motors and universal electrical machines. Creating geometries with a more curious than usual design offers some improvement in certain desirable characteristics with the disadvantage of increasing complexity or degrading other features. Their main difference is in their design geometry which offers some improvement in certain desired functional characteristics [179].

In [180], a machine is designed to increase the torque attributed to the volume of magnets used to implement a gearless motor with high torque at low speeds. The results showed the improvement of the average torque of the proposed machine. The competitiveness of the vernier machine was validated using 2D finite element analysis under the same machine volume as that of the conventional machine.

In Vernier triple rotor axial-flow radial permanent magnet machines (shown Figure 35), a common phenomenon in axial-flow machines is the combination of more than one stator and rotor in order to increase the power and torque produced with a smaller increase in the final volume of the

 doi:10.20944/preprints202312.1678.v1

machine and without the need to create several designs. By appropriately summing a basic machine design two, three or more times the torque and power requirements are achieved. The key feature of these machines is to eliminate disadvantages of Vernier machines while providing high power factor, high power and torque density, high copper utilization and increased efficiency as a consequence [181].

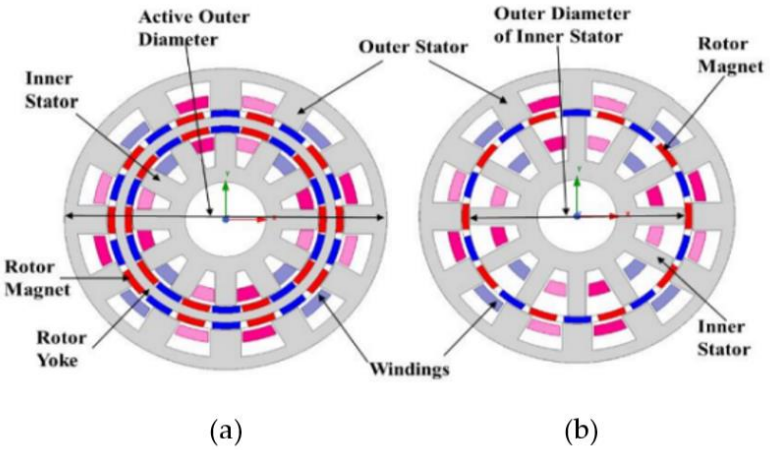

Figure 35. PMVM geometries of radial type with double air gap: (a) with iron body rotor; (b) without iron body rotor [180].

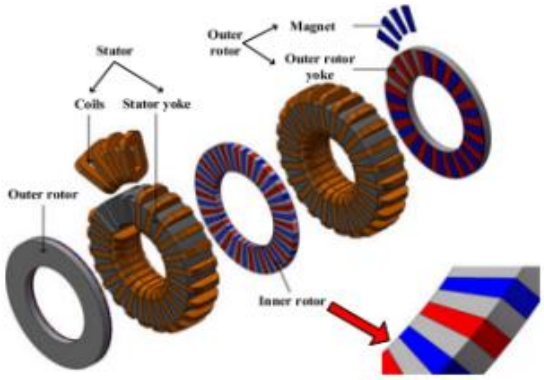

Figure 36. Triple rotor axial flow Vernier machine configuration [181].

Also, a similar methodology is followed for rotor design where in [182] an example of comparison and implementation of two motor rotor designs for an automotive application using ferrites is given. The investigation focused on the use of the non-magnetic material in order to achieve a reduction in demagnetization and an increase in magnetic drag torque by using vacuum triangles in the geometry. The check of demagnetization, mechanical strength, torque ripple with and without load shown in Figure 37 shows that the proposed solution using rare earth free magnets is feasible in real application.

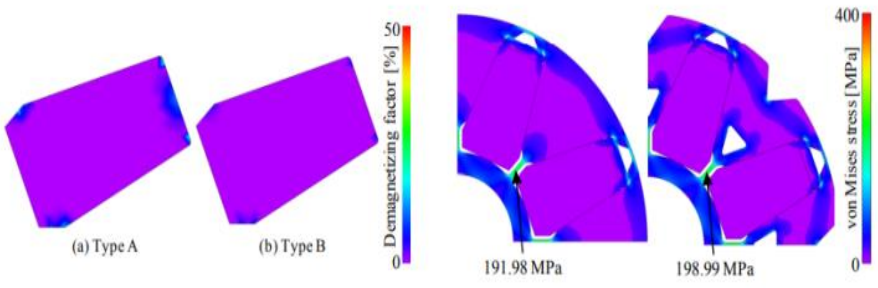

 doi:10.20944/preprints202312.1678.v1

Figure 37. Comparison of the two types A and B in demagnetization effects in magnets and mechanical stress in the rotor [182].

6.3. Case study using Basic 2-D Mechanical Analysis

To investigate the effects of rotor deformation due to centrifugal forces, a mechanical static model has been created which is weakly coupled to a nonlinear internal PM machine. The deformations of the outer rays of the rotor are estimated in a first step using the structural solver and then entered into the electromagnetic solver. Significant impact on the mechanical deformation of the runner which is due to the different V-shaped angles. The higher the maximum deformation, it imposes corresponding mechanical stresses on the magnetic bridges [183].

The mapping of the variables of the V vector to the curvatures in the rotor cases is shown in Figure 38 where the geometry of the motor studied is illustrated. It is worth noting that in the structural analysis model only half of a pole section needs to be drawn, whereas in the electromagnetic model it is necessary to consider a pole section of the rotor geometry. The geometry of the rotor is limited to only one pole, its partitioning is performed by finite element analysis (shown Figure 39), with meshing is dense enough to obtain reliable results without excessive use of computational resources and the consequent requirement for large computational time.

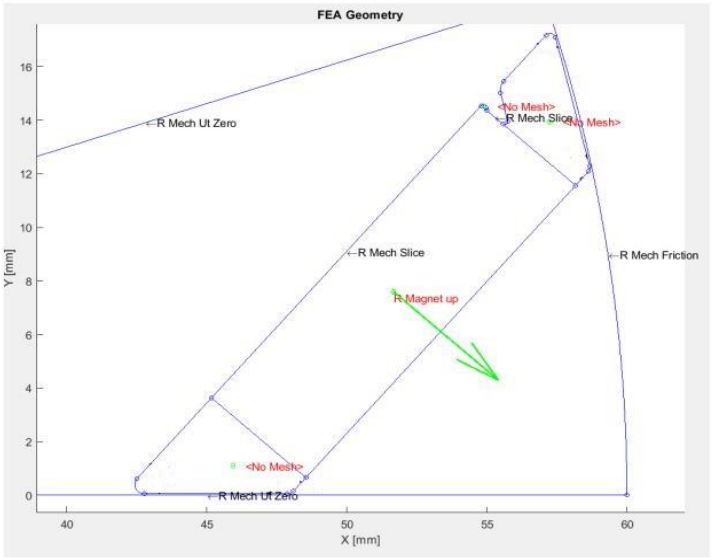

Figure 38. Rotor geometry with mechanical boundary conditions applied along suitable lines.

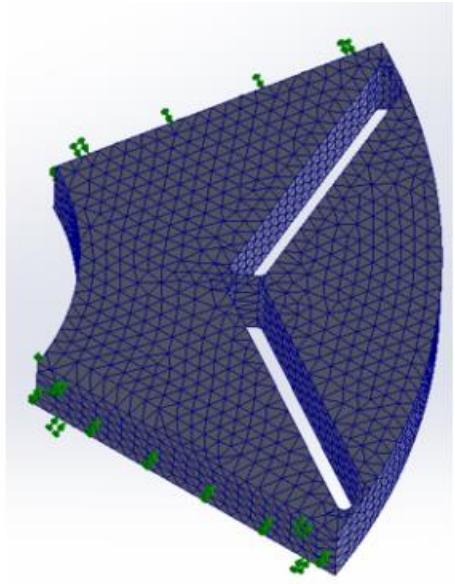

 doi:10.20944/preprints202312.1678.v1

Figure 39. Analysis of rotor geometry in finite elements.

6.3.1. Formulation of the 2D model for Mechanical Analysis

The structural analysis is carried out by developing a mechanical static solver in order to examine 2D plane stresses in isotropic materials. According to the proposed methodology which was based on the Constant Stress Triangle (CST), the matrices representing the Elasticity (E) and the mechanical stresses using the following equations:

$$[D] = \frac{E}{(1-\nu^2)}\begin{bmatrix} 1 & \nu & 0 \\ \nu & 1 & 0 \\ 0 & 0 & \frac{(1-\nu)}{2} \end{bmatrix} \quad (14)$$

$$\varepsilon_x = \frac{dN_1}{dx}u_1 + \frac{dN_2}{dx}u_2 + \frac{dN_3}{dx}u_3 \quad (15)$$

$$\varepsilon_y = \frac{dN_1}{dy}u_1 + \frac{dN_2}{dy}u_2 + \frac{dN_3}{dy}u_3 \quad (16)$$

$$Y_{xy} = \frac{dN_1}{dy}u_1 + \frac{dN_1}{dx}u_1 + \frac{dN_2}{dy}u_2 + \frac{dN_2}{dx}u_2 + \frac{dN_3}{dy}u_3 + \frac{dN_3}{dx}u_3 \quad (17)$$

$$\sigma = [\sigma_{xx} \ \sigma_{yy} \ \sigma_{xy}]^T \quad (18)$$

$$e = [e_{xx} \ e_{yy} \ e_{xy}]^T \quad (19)$$

This model can also support boundary conditions for the air gap slip zone. Such a boundary condition allows avoiding the redesign of the geometry during rotor rotation. The nodes on both the stator side and the rotor side are kept stationary and a zone in the air gap guarantees the inclusion of the motion. This technique constitutes a practical alternative solution for taking into account the rotating mesh in the air gap, compared to analytical solutions of specific elements. In addition, the specific weakly coupled mechanical 2D electromagnetic finite element model can represent permanent magnet materials by determining appropriate values of residual magnetization Br and relative permeability.

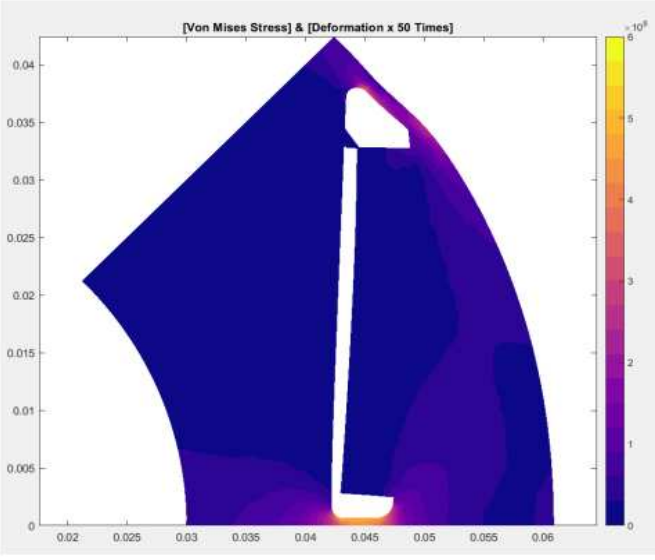

Figure 40. Structural analysis results representing Von-Mises stress distribution and respective deformation under maximum speed conditions (15000Rpm).

 doi:10.20944/preprints202312.1678.v1

The geometry shown in Figure 41 has a thin section that holds the iron section in front of the magnet and iron-bridge positions that connects one pair of poles to the adjacent one in order to limit magnetic scattering in the iron body. It appears that at 3000 rpm for this geometry the maximum stress is 27 MPa with a fracture limit of this type of iron is 470 MPa.

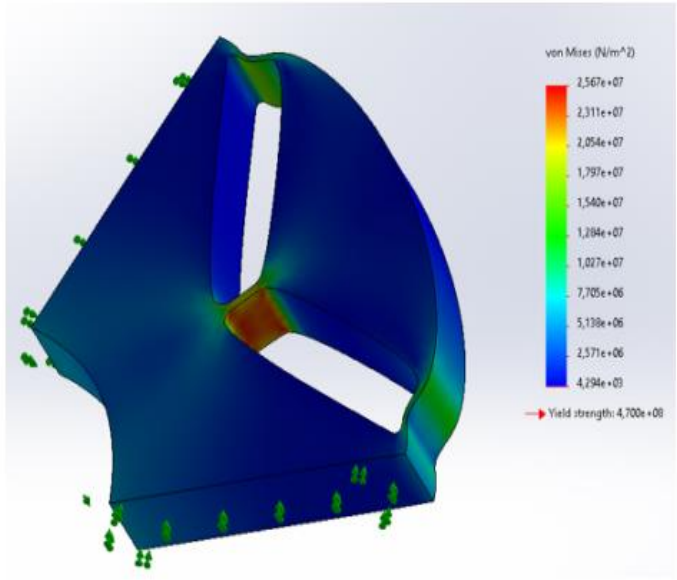

Figure 41. Displacement of iron due to centrifugal force.

6.3.2. Formulation of the 2D Model for Electromagnetic Analysis

The proposed electromagnetic nonlinear weakly coupled mechanical 2D electromagnetic finite element model has been developed to work with 2D triangular grids, considering a given single BH function of the initial magnetization curve that contains nonlinear relative permeability characteristics in each element. The application of the Newton - Raphson algorithm allows accelerating the convergence towards the solution.

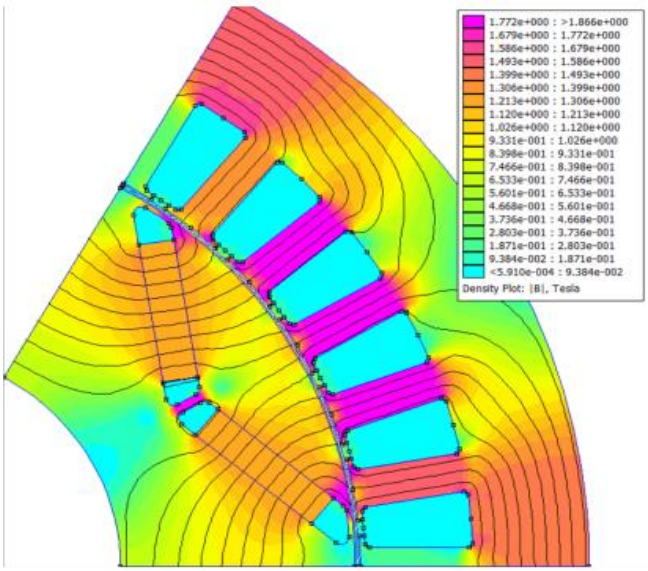

Figure 42. EM-FEA solution results showing flux density module B and equipotential lines under for full loading and angle 111.39^0.

6.3.3. Optimization of Rotor Mass and Leakage Flux

Preprints.org (www.preprints.org) | NOT PEER-REVIEWED | Posted: 22 December 2023 doi:10.20944/preprints202312.1678.v1

Mechanical optimization is performed by developing a certain evolutionary algorithm that optimizes an appropriate objective function. In particular, a genetic algorithm (GA) of 1000 generations with a population size of 100 each is employed. The specific population size ensures, the detection of the total minimum of the cost function for this application, which also converges to 800 generations approximately. With the application of this algorithm, a better convergence of values is achieved, while the parallel application on a computer system can provide a great reduction in computing time. In the case of the considered machine, a variation of the order of a few percent in torque can be obtained under nominal operating conditions at 15000 rpm. The exploration is designed in such a way that we set boundary values of the optimization variables, so that the genetic algorithm knows what boundaries it will fall within in order to make the search for the optimal solution faster.

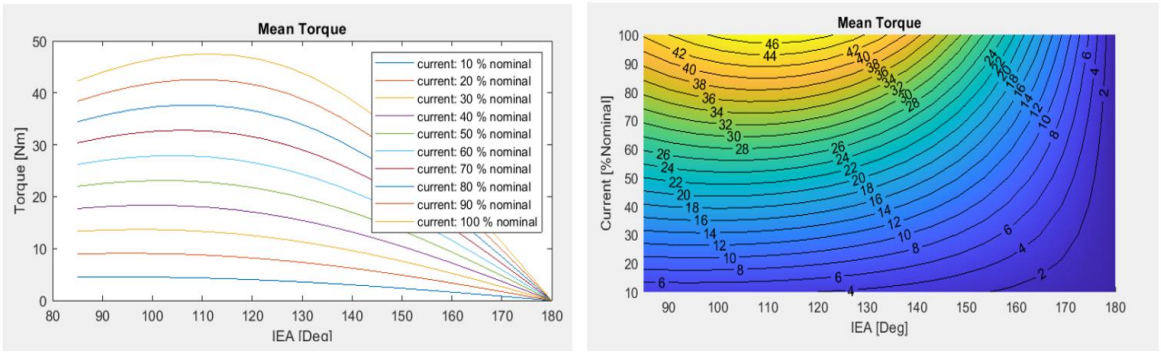

(a) (b)

Figure 43. Average torque graphs as a fuction of: (a) internal torque angle; (b) operating current.

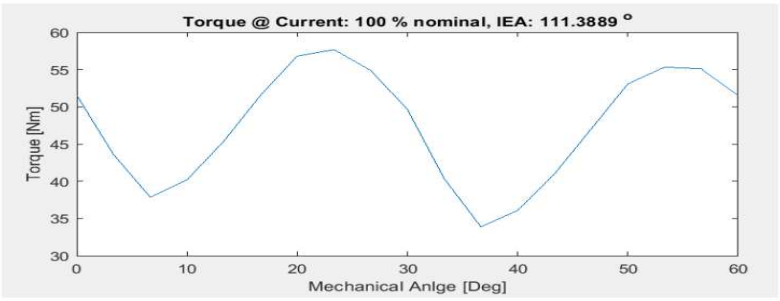

Figure 44. Torque diagram at maximum load as a function of rotor position.

6.3.4. Spatial Harmonics in the Air Gap

We observe differences in the spatial distribution of the flux density and the corresponding harmonics can lead to different iron losses caused by the slot harmonics. The proposed method uses the geometric distortion of the rotor near the gap [184]. This particular type of coupling between electromagnetic and mechanical phenomena results in a reliable numerical method in terms of numerical stability-convergence issues. In general, a large part of the losses of a modern electric motor is due to harmonic losses. By applying an optimized model to visualize and calculate the harmonic iron losses in a IPMSM. The main conclusions are related to harmonic currents and voltage along with saturation and cross-saturation occurrence phenomena. The proposed harmonic dq model includes a harmonic iron loss resistor to calculate the losses at different speeds and loads. The determination of all the above elements highlighted both the accuracy of the model and the more detailed representation of results compared to other conventional loss minimization and maximum torque per ampere techniques [185].

Rotor deflection in high-speed regions is critical and must be taken into account at the design stage in order to avoid exceeding the maximum allowable leakage limit and compromising the reliability of the motor. Particular attention should be paid in the analysis to the effect of the rotor

 doi:10.20944/preprints202312.1678.v1

radius on critical parameters such as air friction losses, rotor and stator heating [186]. In addition, in cases where the mechanical strength of the rotor is not properly ordered by reducing the tensile strength relative to the compressive strength [187], the reduction of its mass can lead to deformations that cause unmeasurable changes in the operating characteristics of the machine. This analysis introduced a methodology to analyze the effects of non-uniform gap deformation, on the characteristics of the permanent magnet motor, due to rotor deformations under high-speed conditions. This technique is based on the weak coupling between mechanical and electromagnetic analysis. It allows a detailed examination of the variations in the harmonics of the spatial flux density, the entangled flux of the stator windings and the electromagnetic torque ripples. It was applied to a machine with internal magnets in a V-type configuration [188].

Based on the harmonic analysis shown in Figures 45 and 46 respectively, an increase in torque after optimization by 20.9% can be observed. Therefore, the dimensions of the machine can be reduced, namely its length by 20% in order to obtain the required torque. The advantage of the proposed method is based on the particular weak coupling adopted to study the interdependent phenomena in this way there is no need to use very powerful computational tools, while its integration into permanent magnet motor design optimization procedures is relatively simple. Consequently, great services can be offered to the designer in terms of high reliability and detailed determination of the variations in operating characteristics at high speeds.

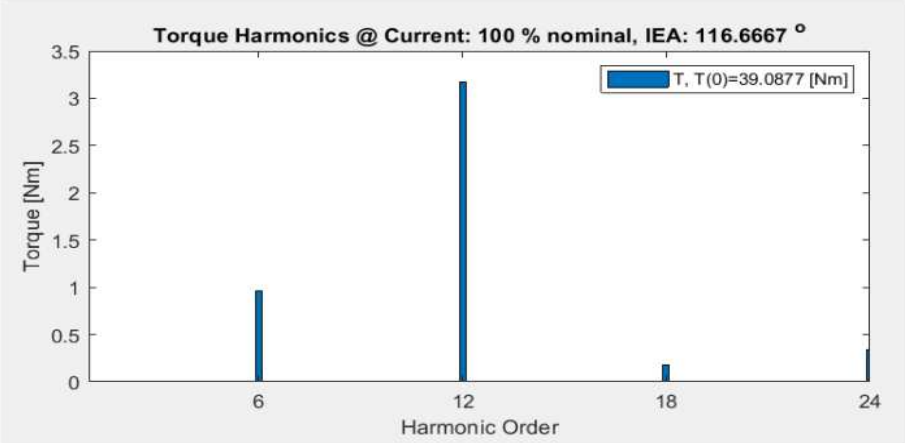

Figure 45. Harmonic content of machine torque before optimisation.

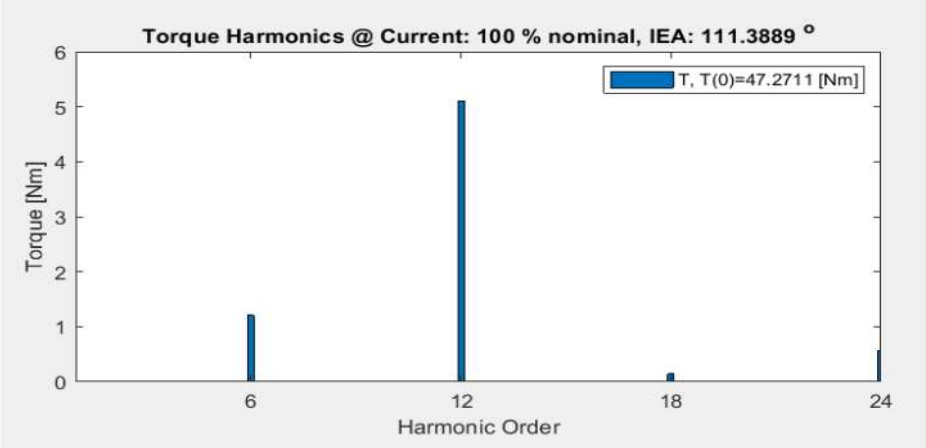

Figure 46. Harmonic content of machine torque after optimisation.

7. Conclusions

The main conclusions drawn from this literature survey concern that the already assessed permanent magnet motor dominant role in low power applications is actually extended to modern

 doi:10.20944/preprints202312.1678.v1

greater power implementations favoring higher speed operation; however, permanent magnet material characteristics present significant variations when operating under harsh conditions and are affected both by temperature rise and mechanical stresses. To that respect demagnetization risks are increased and detailed loss handling has to be considered at the design stage. Consequently, it is necessary to account for the losses in permanent magnets due to high frequency effects caused by space harmonics in case of high rotor rotation speeds as well as by higher harmonic content of converter supplies. Appropriate methodologies have already been developed for analysis of the respective machine operating characteristics, including detailed representation of harmonic losses in the permanent magnets and the surrounding ferromagnetic laminated magnetic circuits as well as combined consideration of the electromagnetic, thermal and mechanical phenomena involved. Respective accurate simulations can be achieved by appropriate weak coupling techniques using methodologies based on the finite element method. It may be noted, that the appropriate permanent magnet material implementation plays a key role in each application, as Neodymium-Iron-Boron alloys, exhibiting higher remanence values, suffer from significant decrease of magnetization with temperature rise, with respect to Samarium-Cobalt alloy rivals, presenting lower saturation magnetization but presenting much better temperature rise withstand. In particular applications, suitable combination of different types of permanent magnet materials may provide effective configuration solutions. Finally, appropriate coupled two dimensional finite element - equivalent circuit equation techniques enable consideration of edge effects in permanent magnet machines by means of reduced computational means, facilitating integration in geometry optimization algorithms and efficient motor design methodologies development.

Author Contributions: Conceptualization, V.I.V. and A.G.K.; methodology, V.I.V. and A.G.K.; software, G.K.S. and F.P.X.; validation, V.I.V., G.K.S., F.P.X., M.S.C.P., T.D.K., M.A.T. and A.G.K.; formal analysis, V.I.V. and A.G.K.; investigation, V.I.V., G.K.S., F.P.X. M.S.C.P., T.D.K., M.A.T. and A.G.K.; data curation, V.I.V., G.K.S., F.P.X. M.S.C.P., T.D.K., M.A.T. and A.G.K.; writing—original draft preparation, V.I.V.; writing—review and editing, A.G.K.; visualization, V.I.V. and A.G.K.; supervision, A.G.K.; project administration, A.G.K.; funding acquisition, V.I.V., G.K.S., M.S.C.P., T.D.K. and A.G.K.; All authors have read and agreed to the published version of the manuscript.

Funding: This research was funded by the European Regional Development Fund of the European Union and Greek National Funds through the Operational Program Competitiveness, Entrepreneurship and Innovation, under the Call RESEARCH-CREATE-INNOVATE under Project T2EDK-00421.

Data Availability Statement: Not applicable.

Conflicts of Interest: The authors declare no conflict of interest.

References

1. Chau, T.K.; Chan, C.C.; Liu, C. Overview of Permanent-Magnet Brushless Drives for Electric and Hybrid Electric Vehicles. *IEEE Trans. Ind. Elect*. **2008**, *55*, 2246-2257.
2. Yang, Y.; He, Q.; Fu, C.; Liao, S.; Tan, P. Efficiency improvement of permanent magnet synchronous motor for electric vehicles. *Ener.* **2020**, *213*,1-11.
3. Lee, C.H.T.; Hua, W.; Long, T.; Jiang, C.; Iyer, L.V.A critical review of emerging technologies for electric and hybrid vehicles. *IEEE Open J. Veh. Techn.* **2021**, *2*, 471-485.
4. Li, C.; Chau, K.T.; Lee, C.H.T.; Song, Z. A critical review of advanced electric machines and control strategies for electric vehicles. *IEEE Proc.* **2021**, *109*, 1004-1008.
5. Wang, Z.; Ching, T.W.; Huang, S.; Wang, H.; Xu, T. Challenges faced by electric vehicle motors and their solutions. *IEEE Acc.* **2020**, *9*, 5228-5249.
6. Yu, Z.; Li, Y.; Jing, Y.; Wang, J. Cooling system of outer rotor SPMSM for a two-seater all-electric aircraft based on heat pipe technology. *IEEE Trans. Tran. Elect.*, **2022**, *8*, 1656-1664.
7. Beniakar, M.E.; Kakosimos, P.E.; Krasopoulos, C.T.; Sarigiannidis, A.G.; Kladas, A.G. Comparison of in-wheel permanent magnet motors for electric traction. In Proceedings of 2014 International Conference on Electrical Machines (ICEM), Berlin, Germany, September 2-5 2014; pp. 2472-2478.
8. Fang, H.; Qu, R.; Li, J.; Zheng, P.; Fan, X. Rotor Design for High-Speed High-Power Permanent-Magnet Synchronous Motor. *IEEE Trans. Ind. Appl.* **2017**, *53*, 3411-3419.
9. Bekka, N.; El H. Zaim, M.El.H.; Bernard, N.; Trichet, D. A novel methodology for optimal design of fractional slot with concentrated windings. *IEEE Trans. En. Con.* **2016**, 31, 1153-1160.

10. Wang, K.; Zhu, Z. Q.; Ombach, G., Torque enhancement of surface-mounted permanent magnet machine using third-order harmonic. *IEEE Trans. Magn.* **2014**, *50*, 2014.
11. Mirahki H.; Moallem M.; Ebrahimi M.; Fahimi B. Asymmetrical magnet shape optimization based on S-C mapping for torque profile mitigation in unidirectional application of SPMS machine. *IEEE Trans. Tran. Elect.* **2019**, *5*, 630-637.
12. Du, Z.S.; Lipo, T.A. High torque density and low torque ripple shaped-magnet machines using sinusoidal plus third harmonic shaped magnets. *IEEE Trans. Ind. Appl.s* **2019**, *55*,2601-2610.
13. Park, H.J.; Lim, M.S.; Lee, C.S. Magnet shape design and verification for SPMSM of EPS system using cycloid curve. *IEEE Acc.* 2019, *7*, 137207-137216.
14. Chabchoud, M.; Salah, I. B.; Krebs, G.; Neji, R.; Marchand, C. PMSM cogging torque reduction: comparison between different shapes of magnet. In Proceedings of 2012 1st International Conference on Renewable Energies and Vehicular Technology, Nabeul, Tunisia, Mar. 26-28, 2012; pp. 206-211.
15. Singh, S.; Pillay, P. Sinusoidal shaped surface permanent magnet motor using cold spray additive manufacturing. In Proceedings of 2020 IEEE Energy Conversion Congress and Exposition (ECCE), Detroit, MI, USA, Oct. 11-15 2020; pp. 2089-2094.
16. Lim, M.S.; Chai, S.H.; Yang, J.S.; Hong, J. P. Design and verification of 150-krpm PMSM based on experiment results of prototype. *IEEE Trans. Ind. Ele.*, **2015**, *62*, 7827-7836.
17. Yoneda, M.; Shoji, M.; Kim, Y.; Dohmeki, H. Novel selection of the slot/pole ratio of the PMSM for auxiliary automobile. In Proceedings of Conference Record of the 2006 IEEE Industry Applications Conference Forty-First IAS Annual Meeting, Tampa, FL, USA, Oct. 8-12, 2006; pp. 8-13.
18. He, C.; Wu, T. Analysis and design of surface permanent magnet synchronous motor and generator. *CES Trans. Electr. Machines and Systems*, **2019**, *3*, 94-100.
19. Chung, S.U.; Kim, J.W.; Chun, Y. D.; Woo, B. C; Hong, D.K. Fractional slot concentrated winding PMSM with consequent pole rotor for a low-speed direct drive: reduction pf rare earth permanent magnet. *IEEE Trans. Energy Convers.* **2015**, *30*, 103-109.
20. Sayed, E.; Yang, Y.; Bilgin, B.; Bakr, M.H.; Emadi, A.A. comprehensive review of flux barriers in interior permanent magnet synchronous machines. *IEEE Acc.* **2019**,*7*, 149168-149181.
21. Liu, G.; Zhai, F.; Chen, Q.; Xu, G. Torque pulsation reduction in fractional-slot concentrated-windings IPM motors by lowering sub-harmonics. *IEEE Trans. Energy Convers.*, 2019, 34, 2084-2095.
22. Kong, Y.; Lin, M.; Jia, L. A novel high power density permanent-magnet synchronous machine with wide speed range. *IEEE Trans. Magn.* **2020**, *56*.
23. Li, J.; Xu, Y.; Zou, J.; Wang, Q.; Liang, W. Analysis and reduction of magnet loss by deepening magnets in interior permanent-magnet machines with a pole/slot ratio of 2/3. *IEEE Trans. Magn.* **2015**, *51*.
24. Sun, X.; Shi, Z.; Lei, G.; Guo, Y.; Zhu, J. Multi-objective design optimization of an IPMSM based on multilevel strategy. *IEEE Trans. Ind. Electr.* **2021**, *68*, 139-148.
25. Ma, Q.; Refaie, El A.; Lequesne, B. Low-cost interior permanent magnet machine with multiple magnet types. *IEEE Trans. Ind. Appl.* **2020**, *56*, 1452-1463.
26. Miyamasu, M.; K. Akatsu, K. An approach to generate high reluctance torque in an inset-type PMSM by square current excitation. In Proceedings of 2012 IEEE International Conference on Power and Energy (PECon), Kota, Kinabalu, Malaysia, December 2-5 2012; pp. 440-445.
27. Gao, P.; Gu, Y.; Shah, H. S.; Abubakar, U.; Wang, X., Calculation and analysis of flux leakage coefficient of interior permanent magnet synchronous motors with fractional slot concentrated windings. *IEEE Trans. Appl. Super.***2019**, *29*.
28. Toulabi, M.S.; Salmon, J.; Knight, A.M. Concentrated winding IPM synchronous motor design for wide field weakening applications. *IEEE Trans. Ind. Appl.* **2017**, *53*, 1892-1900.
29. Toulabi, M.S.; Salmon, J.; Knight, A.M. Concentrated winding IPM synchronous motor design for wide field weakening applications. *IEEE Trans. Ind. Appl*. **2017**, *53*, 1892-1900.
30. Chai, F.; Li, Y.; Liang, P.; Pei, Y. Calculation of the maximum mechanical stress on the rotor of interior permanent-magnet synchronous motors. *IEEE Trans. Ind. Electr*.**2016**, *63*, 3420-3432.
31. Hong, S.G.; Park, II.H. Continuum-sensitivity-based optimization of interior permanent magnet synchronous motor with shape constraint for permanent magnet. *IEEE Trans.Magn.* **2020**, *56*.
32. Lim, H.K.; Song, B.K.; Kim, S.II.; Hong, J.P. A study on the relation between rotor rib and maximum power of IPMSM in flux weakening region. In Proceedings of the 2010 International Conference on Electrical Machines and Systems, Incheon, South Korea, Oct. 10-13, 2010.
33. Chen, Z.; Li, G.A V type permanent magnet motor simulation analysis and prototype test for electric vehicle. *IEEE Acc.* **2019**, *7*, 174839-46.
34. Lee, K.D.; Lee, H.W.; Lee, J.; Kim, W.H. Analysis of motor performance according to the inductance design of IPMSM. *IEEE Trans.Magn.*,**2015**,*51*.

35. Song, I.S.; Lee, C.H.; Kim, K.C. Comparison characteristics according to changing magnet pole-arc of double-layered V-shape IPMSM for large commercial EVs. In Proceedings of 2021 24th International Conference on Electrical Machines and Systems (ICEMS), Gyeongju, Kora, Oct. 31 – Nov. 3 2021.
36. Dong, J.; Gu, A.; Yang, M.; Zhang, D. A method for improving torque performances of IPMSM. In Proceedings of 8th International Conference on Power Electronics Systems and Applications (PESA), Hong Kong, China, Dec. 7-10 2020.
37. Ma, C.; Li, J.; Zhao, H.; Wang, J.; Yin, X.; Zuo, S.; Wu, X.; Lu, H. 3-D analytical model of armature reaction field of IPMSM with multi-segmented skewed poles and multi-layered flat wire winding considering current harmonics. *IEEE Acc.* **2020**, *8*, 151116-1511124.
38. Zuopeng, D.; Bing, Z.; Dejun, ϒ. A design of fractional-slot concentrated winding IPM synchronous motor for electric vehicle. In Proceedings of IECON 2017 – 43rd Annual Conference of the IEEE Industrial Electronics Society, Beijing, China, Oct. 29 – Nov. 1 2017.
39. Park, S.H.; Chin, J.W.; Cha, K.S.; Ryu, J.Y.; Lim, M.S. Characteristic analysis of IPMSM for EV traction considering the effect of field and armature excitations on AC copper loss. In Proceedings of 2021 IEEE Energy Conversion Congress and Exposition (ECCE). Vancouver, BC, Canada, Oct. 10-14, 2021; pp. 4486-4491.
40. Kim, Y.K.; Jeong, L.J.; Rhyu, S.H.; Jung, I.S. A study on permanent magnet synchronous motor for neighborhood electric vehicle. In Proceedings of 2012 IEEE Vehicle Power and Propulsion Conference, Seoul, South Korea, Oct. 9-12, 2012; pp. 1081-1085.
41. Kim, M.J.; Lee, K.D.; Lee, J.J.; Han, G.H.; Jeong, T.C.; Kim W.H.; Koo D.H.; Lee J. Torque density elevation in concentrated winding interior PM synchronous motor with minimized magnet volume. *IEEE Trans. Magn.* **2013**, *49*, 3334-3337.
42. Hao, J.; Suo, S.; Yang, Y.; Wang, Y.; Wang W.; Chen X. Optimization of torque ripples in an interior permanent magnet synchronous motor based on the orthogonal experimental method and MIGA and RBF neural networks. *IEEE Acc*. **2020**, *8*, 27202-27209.
43. Galioto S.J.; Reddy P.B.; El-Refaie A.M.; Alexander J.P. Effect of magnet types on performance of high-speed spoke interior-permanent-magnet machines designed for traction applications. *IEEE Trans. Ind. Appl.* **2015**, *51*, 2148-2160.
44. Fatemi A.; Ionel D.M.; Popescu M.; Chong Y.C.; Demerdash, N.A.O. Design optimization of a high torque-density spoke-type PM motor for a formula E race drive cycle. *IEEE Trans. Ind. Appl*. **2018**, *54*, 4343-4354.
45. Kim, K.-C. A novel method for minimization of cogging torque and torque ripple for interior permanent magnet synchronous motor. *IEEE Trans. Magn.* **2014**,*50*.
46. Hwang, K.Y.; Jo, J.H.; Kwon, B.I. A study on optimal pole design of spoke-type IPMSM with concentrated winding for reducing the torque ripple by experiment design method. *IEEE Trans. Magn.* **2009**, *45*, 4712-4715.
47. Wang, J.; Geng, W.; Li Q.; Li L.; Guo J. A novel spoke-type IPM rotor with hybrid radial and axial flux concentration for reduction of interpolar leakage flux. *IEEE Trans. Magn.* **2022**, *58*.
48. Hemmati, R.; Vahid, S.; EL-Refaie, A. A novel design for a high specific power interior permanent magnet machine for aerospace applications. In Proceedings of 2020 IEEE Energy Conversion Congress and Exposition (ECCE), Detroit, MI, USA, Oct. 11-15, 2020; pp. 1735-1742.
49. Cui, W.; Wang, D.; Ren, L.; Zhang, Y. A new optimized IPMSM for EVs with reduced magnet loss for over-modulation operation. *IEEE Trans. Magn.* **2023**, *59*.
50. Kim, S.II.; Kim, Y.K.; Lee, G.H.; Hong, J.P. A novel rotor configuration and experimental verification of interior PM synchronous motor for high-speed applications. *IEEE Trans. Magn.* **2012**, *48*, 843-846.
51. Choi, G.; Bramerdorfer, G. Comprehensive design and analysis of an interior permanent magnet synchronous machine for light-duty passenger EVs. *IEEE Acc.* **2021**, *10*, 819-831.
52. Jung, Y.H.; Park, M.R.; Kim, K.-O.; Chin J.W.; Hong J.P.; Lim M.S. Design of high-speed multilayer IPMSM using ferrite PM for EV traction considering mechanical and electrical characteristics. *IEEE Trans. Ind. Appl.* **2021**, *57*,327-339.
53. Cao, Z.; Liu, J. Cogging torque reduction for outer rotor interior permanent magnet synchronous motor. In Proceedings of IECON 2020 46th Annual Conference of the IEEE Industrial Electronics Society, Singapore, Oct. 18-21 2020; pp. 2689-2693.
54. Yu, D.; Huang, X.; Zhang, X.; Zhang, J.; Lu, Q.; Fang, Y. Optimal design of outer rotor interior permanent magnet synchronous machine with hybrid permanent magnet. *IEEE Trans. Appl. Super*. **2019**, *29*.
55. Nakata, T.; Sanada, M.; Morimoto, S.; Inoue, Y. Automatic design of IPMSMs using a genetic algorithm combined with the coarse-mesh FEM for enlarging the high-efficiency operation area. *IEEE Trans. Ind. Electr.* **2017**, *64*,9721-9728,

56. Lee, Y.G.; Bang, T.K.; Woo, J.H.; Jo, S.T.; Choi, J.Y. Comparative study of mechanical and electromagnetic aspects of interior permanent magnet synchronous motor according to the rotor shapes. In Proceedings of 2021 24th International Conference on Electrical Machines and Systems (ICEMS), Gyeongju, Korea, Oct. 31 – Nov. 3, 2021; pp. 1279-1283.
57. Yoshida, Y.; Yanagisawa, T.; Tajima, K. Consideration of asymmetrical magnetic pole IPMSM using bonded rare-earth magnet. In Proceedings of 2020 23rd International Conference on Electrical Machines and Systems (ICEMS), Hamamatsu, Japan, Nov. 24-27, 2020; pp. 720-723.
58. Asef, P.; Denai,M.; Marques, B.R.; Paulides J.J.H.; Lapthorn, A. Commutation angle maps evaluation for magnet arrangements of interior permanent magnet synchronous machines in electric vehicles. In Proceedings of 2021 International Conference on Smart Energy Systems and Technologies (SEST), Vaasa, Finland, Sept. 6-8, 2021.
59. Guo, Y.; Liu, L.; Ba, X.; Lu, H.; Lei, G.; Yin W.; Zhu J. Designing High-Power-Density Electric Motors for Electric Vehicles with Advanced Magnetic Materials. *World Elec. Veh. J.* 2023, 14(4), pp. 1-21.
60. Pechlivanidou, M.S.C; Kladas A.G. Tree-Dimensional- Printed Magnetic Iron Material Modelling for High Speed Actuators. *IEEE Trans. Magn.*, **2023**, *59*.
61. Yu, G.; Huang, J.; Xiao, J.; Xu, Y.; Zou, J. Effect of High-Pressure Environment on Deep-Sea Permanent Magnet Synchronous Motors With Fe-Co-V Alloy. *IEEE Trans. Magn.* **2023**, *59*.
62. Manolas, I.; Kladas, A.; Svechkarenko, D.; Chin, R. Magnetization Regulation in Variable Flux PM-Assisted Synchronous Reluctance Machines. In Proceedings of 2018 XIII International Conference on Electrical Machines (ICEM), Alexandroupoli, Greece, 03-06 September 2018, pp. 2224-2228.
63. Tsunata, R.; Takemoto, M.; Ogasawara, S.; Orikawa, K. A Proposal of a Delta-Type Salient Pole Variable Flux Memory Motor Having Large Flux Barrier for Traction Applications. In Proceedings of 2019 IEEE Energy Conversion Congress and Exposition (ECCE), Baltimore, MD, USA, 29 Sept.- 03 October 2019, pp. 6054-6061.
64. Nair, S.S.; Patel, V.I.; Wang, J. Post-Demagnetization Performance Assessment for Interior Permanent Magnet AC Machines. *IEEE Trans. Magn.* **2016**, *52*.
65. Jeong, C.-L.; Hur, J. Optimization Design of PMSM with Hybrid-Type Permanent Magnet Considering Irreversible Demagnetization. *IEEE Trans. Magn.* **2017**, *53*.
66. Faiz, J.; Mazaheri-Tehrani, E. Demagnetization Modeling and Fault Diagnosing Techniques in Permanent Magnet Machines Under Stationary and Nonstationary Conditions: An Overview. *IEEE Trans. Ind.* Appl., **2017**, *53*, 2772-2785.
67. De Bisschop, J.; Sergeant, P.; Hemeida, A.; Vansompel, H.; Dupré L. Analytical Model for Combined Study of Magnet Demagnetization and Eccentricity Defects in Axial Flux Permanent Magnet Synchronous Machines. *IEEE Trans. Magn.* **2017**, *53*.
68. Reigosa, D.; Fernández, D.; Martínez, M.; Park, Y.; Lee, S.B.; Briz, F. Permanent Magnet Synchronous Machine Non-Uniform Demagnetization Detection Using Zero-Sequence Magnetic Field Density. *IEEE Trans. Ind. Appl.* 2019, 55, 3823-3833.
69. Mörée, G.; Sjölund, J.; Leijon, M. A Review of Permanent Magnet Models Used for Designing Electrical Machines. *IEEE Trans. Magn.* **2022**, *58*, pp. 1-19.
70. Hamidizadeh, S.; Alatawneh, N.; Chromik, R.R.; Lowther D.A. Comparison of different demagnetization models of permanent magnet in machines for electric vehicle application. *IEEE Trans. Magn.* **2016**, *52*, 1–4.
71. Moosavi, S.S; Djerdir, A.; Amirat, Y.A.; Khaburi,D.A. Demagnetization fault diagnosis in permanent magnet synchronous motors: A review of the state-of-the-art. *J. Magn. Magn. Mater.* **2015**, *391*, pp. 203–212.
72. Uršič, L.; Nemec M. Permanent magnet synchronous machine demagnetisation prevention and torque estimation control considering rotor temperature. *IET Power Electron.* **2019**, *12*, 2161–2169.
73. Leuning, N.; Elfgen, S.; Groschup, B.; Bavendiek, G.; Steentjes, S.; Hameyer, K. Advanced soft- and hard-magnetic material models for the numerical simulation of electrical machines. *IEEE Trans. Magn.* **2018**, *54*, 1–8.
74. Ruoho, S.; Dlala, E.; Arkkio, A. Comparison of Demagnetization Models for Finite-Element Analysis of Permanent-Magnet Synchronous Motor. *IEEE Trans. Magn.* **2007**, *43*, 3964-3968.
75. Choi, G. Analysis and Experimental Verification of the Demagnetization Vulnerability in Various PM Synchronous Machine Configurations for an EV Application. *Energ.* **2021**, *14*, 1-16.
76. De Bisschop, J.; Sergeant, P.; Hemeida, A.; Vansompel, H.; Dupre, L. Analytical Model for Combined Study of Magnet Demagnetization and Eccentricity Defects in Axial Flux Permanent Magnet Synchronous Machines. *IEEE Trans. Magn.* **2017**, *53*, 8107712.
77. Reigosa, D.; Fernandez, D.; Martinez, M.; Park, Y.; Lee, S.B.; Briz, F. Permanent Magnet Synchronous Machine Non-Uniform Demagnetization Detection Using Zero-Sequence Magnetic Field Density. *IEEE Trans. Ind. Appl.* **2017**,*55*, 3823-3833.

78. Lee, S.T. Demagnetization study of an interior permanent magnet synchronous machine considering transient peak 3 phase short circuit current. In Proceedings of 2017 Annual Conference of the IEEE Energy Conversion Congress and Exposition (ECCE), Cincinnati, USA, 01-05 October 2017, pp. 4694-4698.
79. Krichen, M.; Elbouchikhi, E.; Benhaji, N.; Chaieb, M.; Benbouzid, M.; Neji, R. Motor Current Signature Analysis-Based Permanent Magnet Synchronous Motor Demagnetization Characterization and Detection. *Mach.* **2020**, *8*, 1-29.
80. Dobzhanskyi, O.; Grebenikov, V.; Gouws, R.; Gamaliia, R.; Hossain, E. Comparative Thermal and Demagnetization Analysis of the PM Machines with Neodymium and Ferrite Magnets. *Ener.* **2022**, *15*, 1-15.
81. Wang, J.; Wang, W.; Atallah, K.; Howe, D. Demagnetization Assessment for Three-Phase Tubular Brushless Permanent-Magnet Machines. *IEEE Trans. Magn.* **2008**, *44*, 2195-2203.
82. Sjokvist, S.; Eriksson, S. Investigation of Permanent Magnet Demagnetization in Synchronous Machines during Multiple Short-Circuit Fault Conditions. *Ener.* **2017**, *10*, 1-12.
83. Baranski, M.; Szelag, W.; Lyskawinski, W. Analysis of the Partial Demagnetization Process of Magnets in a Line Start Permanent Magnet Synchronous Motor. *Ener.* **2020**, *13*, 1-20.
84. Zhou, P.; Lin, D.; Xiao, Y.; Lambert, N.; Rahman, M.A. Temperature-Dependent Demagnetization Model of Permanent Magnets for Finite Element Analysis. *IEEE Trans. Magn.* **2012**, *48*, 1031-1034.
85. Li Z.; Huang, X.; Xu, X.; Chen, Z.; Jiang, Z.; Wu, L.; Shi, T.; Zhang, J. Nonlinear Analytical Model for Predicting Magnet Loss in Surface-Mounted Permanent-Magnet Motors. *IEEE Trans. Magn.* **2022**, *58*, 8203705.
86. Ouamara, D.; Dubas, F. Permanent-Magnet Eddy-Current Losses: A Global Revision of Calculation and Analysis. *Math. and Comput. Appl.* **2019**, *24*, p. 67.
87. Egorov, D.; Petrov, I.; Pyrhönen J.J.; Link, J.; Stern, R.; Sergeant, P.; Sarlioglou, B. Hysteresis Loss in NdFeB Permanent Magnets in a Permanent Magnet Synchronous Machine. *IEEE Trans. Ind. Electr.* **2022**, *69*, pp. 121–129.
88. Wu, L.J.; Zhu, Z.Q.; Staton, D.; Popescu, M.; Hawkins, D. Analytical Model for Predicting Magnet Loss of Surface-Mounted Permanent Magnet Machines Accounting for Slotting Effect and Load. *IEEE Trans. Magn.* **2012**, 48, 107-117.
89. Mirzaei, M.; Binder, A.; Funieru, B.; Susic, M. Analytical Calculations of Induced Eddy Currents Losses in the Magnets of Surface Mounted PM Machines With Consideration of Circumferential and Axial Segmentation Effects. *IEEE Trans. Magn.* **2012**, *48*, 4831-4841.
90. Zhang, D.; Ebrahimi, A.; Wonlers, C.; Redlich, J.; Ponick, B. On the analytical calculation of eddy-current losses in permanent magnets of electrical motors. In Proceedings of 2020 Annual Conference of the IEEE Industrial Electronics Society (IECON), Baltimore, Singapore, 18-21 October 2020, pp. 1052-1056.
91. Nair, S.S.; Wang, J.; Sun, T.; Chen, L.; Chin, R.; Beniakar, M.; Svechkarenko, D.; Manolas, I. Experimental Validation of 3-D Magnet Eddy Current Loss Prediction in Surface-Mounted Permanent Magnet Machines. *IEEE Trans. Magn.* **2017**, *53*, 4380-4388.
92. Davarpanah, G.; Faiz, J. Nonlinear Modelling of a C-Core Connected Two-Phase Switched Reluctance Motor. *IEEE Trans. Ener. Conver.* **2021**, *36*, pp. 2761–2769.
93. Li, H.; Wang, L.; Li, J.; Zhang, J. An Improved Loss-Separation Method for Transformer Core Loss Calculation and Its Experimental Verification. *IEEE Acc.* **2020**, *8*, 204847-204854.
94. Ionel, D.M.; Popescu, M.; Dellinger, S.J.; Miller, T.J.E.; Heideman, R.J.; McGilp, M.I. On the variation with flux and frequency of the core loss coefficients in electric machines. *IEEE Trans. Ind. Appl*. **2006**, *42*, 658-667.
95. Boglietti, A.; Cavagnino, A.; Ionel, D.M.; Popescu, M.; Staton, D.A.; Vaschetto, S. A General model to predict the iron losses in inverter fed induction motors. In Proceedings of 2009 IEEE Energy Conversion Congress and Exposition, San Jose, USA, 20-24 September 2009, pp. 1067-1074.
96. Sirimanna, S.; Balachandran, T.; Haran, K. A Review on Magnet Loss Analysis, Validation, Design Considerations, and Reduction Strategies in Permanent Magnet Synchronous Motor. *Ener.* **2022**, *15*, 1-16.
97. Huang, W.Y., Bettayeb, A.; Kaczmarek, R.; Vannier, J.C. Optimization of Magnet Segmentation for Reduction of Eddy-Current Losses in Permanent Magnet Synchronous Motor. *IEEE Trans. Energy Convers*. **2010**, *25*, 381-387.
98. Belahcen, A.; Arkkio, A. Permanent magnets models and losses in 2D FEM simulation of electrical machines. In Proceedings of International Conference on Electrical Machines (ICEM), Rome, Italy, 06-08 September 2010.
99. Steentjes, S.; Boehmer, S.; Hameyer, K. Permanent Magnet Eddy-Current Losses in 2-D FEM Simulations of Electrical Machines. *IEEE Trans. Magn.*, **2015**, *51*, 6300404.

100. Sain, C.; Banerjee, A.; Biswas, P.K. Modelling and comparative dynamic analysis due to demagnetization of a torque controlled permanent magnet synchronous motor drive for energy-efficient electric vehicle. *ISA Trans.* **2019**, *97*.
101. Park, H.S.; Jeung, T.C.; Lee, J.K.; Lee, B.K. Analysis on Harmonic Loss of IPMSM for the Variable DC-link Voltage through the FEM-Control Coupled Analysis. *J. Elect. Eng. Techn.*, **2016**, *12*, 225-229.
102. Ruoho, S.; Santa-Nokki, T.; Kolehmainen, J.; Arkkio, A. Modeling Magnet Length In 2-D Finite-Element Analysis of Electric Machines. *IEEE Trans. Magn.*, **2009**, *45*, 3114-3120.
103. Almandoz, G.; Poza, J.; Rodriquez, M.A.; Gonzalez, A. Analytic model of a PMSM considering spatial harmonics. In Proceedings of International Symposium on Power Electronics, Electrical Drives, Automation and Motion, Ischia, Italy, 11-13 June 2008, pp. 603-608.
104. Pyrhonen, J.; Jussila, H.; Alexandrova, Y.; Rafajdus, P.; Nerg, J. Harmonic Loss Calculation in Rotor Surface Permanent Magnets-New Analytic Approach. *IEEE Trans. Magn.*, **2012**, *48*, 2358-2366.
105. Sergeant, P.; Van den Bossche, A. Segmentation of Magnets to Reduce Losses in Permanent-Magnet Synchronous Machines. *IEEE Trans. Magn.*, **2008**, *44*, 4409-4412.
106. Tessarolo, A. A survey of state-of-the-art methods to compute rotor eddy-current losses in synchronous permanent magnet machines. In Proceedings of IEEE Workshop on Electrical Machines Design, Control and Diagnosis (WEMDCD), Nottingham, UK, 20-21 April 2017, pp. 12-19.
107. Fitouri, M.; Bensalem, Y.; Naceur, A.M. Modeling and detection of the short-circuit fault in PMSM using Finite Element Analysis. *IFAC-PapersOnline*. **2016**, *49*, 1418-1423.
108. Amrhein, M.; Krein, P.T. Magnetic Equivalent Circuit Simulations of Electrical Machines for Design Purposes. In Proceedings of IEEE Electric Ship Technologies Symposium, Arlington, USA, 21-23 May 2007, pp. 254-260.
109. NGUYEN, G.M.T.; Denis, N.; Wu, Y.; Odawara, S. Study of the Effect of Load Torque on the Iron Losses of Permanent Magnet Motors by Finite Element Analysis. *IEEJ J. Ind. Appl.* **2019**, *8*, 522-531.
110. El Hadraoui, H.; Zegrari, M.; Chebak, A.; Laayati, O.; Guennouni, N. A Multi-Criteria Analysis and Trends of Electric Motors for Electric Vehicles. *World Electr. Veh. J.* **2022**, *13*,1-28.
111. Sizov, G.Y.; Ionel, D.M.; Demerdash, N.A.O. Modeling and Parametric Design of Permanent-Magnet AC Machines Using Computationally Efficient Finite-Element Analysis. *IEEE Trans. Ind. Electr.* **2012**, *59*, 2403-2413.
112. Dubas, F.; Rahideh, A. Two-Dimensional Analytical Permanent-Magnet Eddy-Current Loss Calculations in Slotless PMSM Equipped With Surface-Inset Magnets. *IEEE Trans. Magn.*, **2014**, *50*, 54-73.
113. Mendonca, G.A.; Maia, T.A.C.; Filho, B.J.C. Magnetic Field Analytical Solution for Non-homogeneous Permeability in Retaining Sleeve of a High-Speed Permanent-Magnet Machine. *Math. and Compita. Appl*. 2018, *23*, 1-16.
114. Woo, J.H.; Bang, T.K.; Lee, H.K.; Kim, K.H.; Shin, S.H.; Choi, J.Y. Electromagnetic Characteristic Analysis of High-Speed Motors With Rare-Earth and Ferrite Permanent Magnets Considering Current Harmonics. *IEEE Trans. Magn.*, **2021**, *57*, 8201805.
115. Faiz, J.; Mazaheri-Tehrani, E. Demagnetization modeling and fault diagnosing techniques in permanent magnet machines under stationary and non-stationary conditions: an overview. *IEEE Trans. Ind. Appl*. **2017**, *53*, 2772-2785.
116. Sakkas, G.; Kladas, A. Design considerations for cost effective Radial Flux Interior Permanent Magnet Motors with increased Demagnetization Robustness. In Proceedings of 2021 IEEE Workshop on Electrical Machines Design, Control and Diagnosis (WEMDCD), Modena, Italy, 08-09 April 2021; pp. 58-63.
117. Jun, P.; Yifeng, L.; Weiye, L. Calculate for Inverter supplied Permanent Magnet Synchronous Motor losses. In Proceedings of 2020 IEEE Vehicle Power and Propulsion Conference (VPPC), Gijon, Spain, 18 November-16 December 2020.
118. Ding, X.; Mi, C. Modeling of eddy current loss in the magnets of permanent magnet machines for hybrid and electric vehicle traction applications. In Proceedings of 2009 IEEE Vehicle Power and Propulsion Conference, Dearborn, USA, 07-10 September 2009.
119. Nair, S.; Wang, J.; Sun, T.; Chen, L.; Chin R.; Beniakar, M.; Svechkareno, D.; Manolas I. Experimental Validation of 3-D Magnet Eddy Current Loss Prediction in Surface-Mounted Permanent Magnet Machines. *IEEE Trans. Ind. Appl.* **2017**, *53*, 4380–4388.
120. Li, Z.; Huang, X.; Xu, X.; Chen, Z.; Jiang, Z.; Wu, L.; Shi, T.; Zhang, J. Nonlinear Analytical Model for Predicting Magnet Loss in Surface Mounted Permanent-Magnet Motors. *IEEE Trans. Magn.* **2022**, *58*,8203705.
121. Sayed, E.; Yang, Y.; Bilgin, B.; Bakr, M.H.; Emadi, A. A Comprehensive Review of Flux Barriers in Interior Permanent Magnet Synchronous Machines. *IEEE Acc.* **2019**, *7*, 149168–149181.

122. Yamazaki, K.; Takaki, Y. Iron Loss Analysis of Permanent Magnet Motors by Considering Minor Hysteresis Loops Caused by Inverters. *IEEE Trans. Magn.* **2019**, *55*, 1300304.
123. Kim, D.M.; Kim, H.H.; Lee, S.G.; Park, M.R.; Lee G.H.; Lim M.S. Estimation Method for Rotor Eddy Current Loss in Ultrahigh-Speed Surface-Mounted Permanent Magnet Synchronous Motor. *IEEE Trans. Magn.* **2021**, *57*, 8103205.
124. Sakkas, G.K.; Kladas, A.G. Particular Model for Efficient Switching Frequency Loss consideration in Surface Mounted Permanent Magnets. *Trans. Magn.* **2023**, *59*.
125. Xue, S.; Feng, J.; Guo, S.; Chen, Z.; Peng, J.; Chu, W.Q.; Huang, L.R.; Zhu, Z.Q. Iron Loss Model Under DC Bias Flux Density Considering Temperature Influence. *IEEE Trans. Magn.* **2017**, *53*, 1–4.
126. Zhao, H.; Ragusa, C.; De la Barriere, O.; Khan, M.; Appino, C.; Fiorillo, F. Magnetic Loss Versus Frequency in Non-Oriented Steel Sheets and Its Prediction: Minor Loops, PWM, and the Limits of the Analytical Approach. *IEEE Trans. Magn.* **2017**, *53*, 1–4.
127. Pietrzak, P.; Wolkiewicz, M.; Demagnetization Fault Diagnosis of Permanent Magnet Synchronous Motors Based on Stator Current Signal Processing and Machine Learning. *Sensors.* **2023**, *23*, 1-26.
128. Sakkas, G.K.; Vasilopoulos, C.R.C.; Bourchas, K.G.; Kladas, A.G. Advanced Design of PWM Inverter Fed Permanent Magnet Motors. *IEEE Trans. Magn.* **2023**, *49*, 8204711.
129. Park, H.J.; Lee, J.G.; Jung, H.-K.; Woo, D.-K. Improved Quasi-3D finite element method for an axial flux permanent magnet motor. In Proceedings of 2016 IEEE Conference on Electromagnetic Field Computation (CEFC), Miami, USA, 13-16 November 2016; pp. 1-1.
130. Hu, Q.; Chen, W.; Hu, Y.; Zhu, X.; Li, B. Asymptotic Boundary Conditions for the Finite Element Modeling of Axisymmetric Period Permanent Magnet Structures. In Proceedings of 2017 18th International Vacuum Electronics Conference (IVEC), London, UK, 24-26 April 2017, pp. 1-2.
131. Liu, X.; Fu, W.N. A Dynamic Dual-Response-Surface Methodology for Optimal Design of a Permanent-Magnet Motor Using Finite-Element Method. *IEEE Trans. Magn.* **2016**, *52*, 1-4.
132. Schmidt, E.; Sušić, M. Parameter evaluation of permanent magnet synchronous machines with tooth coil windings using the frozen permeabilities method with the finite element analyses. In Proceedings of 2012 25th IEEE Canadian Conference on Electrical and Computer Engineering (CCECE), Montreal, Canada, 29 April-02 May 2012.
133. Franco de Assis, L.; Lemes Filho, C.-C.; Teixeira de Paula, G.; Pinheiro de Alvarenga B. Comparative Analysis of Different Methods Associated to the Frozen Permeability Method for On-Load Cogging Torque Evaluation in Permanent Magnet Synchronous Machines. *IEEE Latin America Trans.* **2021**, *19*, 199-207.
134. Neumann, J.; Henaux, C.; Fadel, M.; Prieto, D.; Fournier, E.; Tientcheu Yamdeu, M. Improved dq model and analytical parameters determination of a Permanent Magnet Assisted Synchronous Reluctance Motor (PMa-SynRM) under saturation using Frozen Permeability Method. In Proceedings of 2020 IEEE International Conference on Electrical Machines (ICEM), Gothenburg, Sweden, 23-26 August 2020, pp. 481-487.
135. Zhong, H.; Peng, B.; Chen, A.; Wang, Y. Primary Iron Loss Analysis on Tubular Permanent Magnet Linear Motor. In Proceedings of 2018 IEEE 4th Southern Power Electronics Conference (SPEC), 2018.
136. Xie, B.; Zhang, Y.; Wang, J.; Liang, B.; Zhang, F. An efficient multidisciplinary design research for the integrated low speed permanent magnet motor system based on analytical and numerical hybrid analysis. *Energy Reports*, **2022**, *8*, 199-208.
137. Chen, Y.; Zhou, J.; Fang, Y.; Gao, Y.; Xia, Y. Multi-field coupling finite-element analysis of the temperature rise in permanent magnet synchronous motor applied for high speed train. In Proceedings of 2016 19th International Conference on Electrical Machines and Systems (ICEMS), Chiba, China,13-16 November 2016.
138. Fu, D.; Xu, Y.; Gillon, F.; Gong, J.; Bracikowski, N. Presentation of a Novel Transverse-Flux Permanent Magnet Linear Motor and Its Magnetic Field Analysis Based on Schwarz–Christoffel Mapping Method. *IEEE Trans. Magn.* **2018**, *54*, 1-4.
139. Nakata, T.; Sanada, M.; Morimoto, S.; Inoue, Y. Automatic design of IPMSMs using a GA coupled with the coarse-mesh finite element method. In Proceedings of 2016 19th International Conference on Electrical Machines and Systems (ICEMS), Chiba, China,13-16 November 2016.
140. Xie, B.; Zhang, Y.; Wang, J.; Liang, B.; Zhang, F. An efficient multidisciplinary design research for the integrated low speed permanent magnet motor system based on analytical and numerical hybrid analysis. *Ener. Repor.* **2022**, *8*, 199-208.
141. Liu, C.; Dong, R.; Ye, B. Comprehensive sensitivity analysis and multi-objective optimization on a permanent magnet linear generator for wave energy conversion. *Renewable Ener.* **2022**, *8*, 841-850.
142. Meo, S.; Zohoori, A.; Vahedi, A. Optimal design of permanent magnet flux switching generator for wind applications via artificial neural network and multi-objective particle swarm optimization hybrid approach. *Energy Conv. and Manag.* **2016**, *110*, 230-239.

143. Gerada, A.; Mebarki, A.; Brown, N.L.; Gerada, C.; Cavagnino, A.; Boglietti, A. High-Speed Electrical Machines: Technologies, Trends, and Developments. *IEEE Trans. Ind. Elect.* **2014**, *61*, 2946–2959.
144. Kindl, V.; Cermak, R.; Ferkova, Z.; Skala, B. Review of Time and Space Harmonics in Multi-Phase Induction Machine. *Ener.* **2020**, *13*, 1-17.
145. Hezzi, A.; Elghali, S.B.; Salem, Y.B.; Abdelkrim, M.N. Control of five-phase PMSM for electric vehicle application. . In Proceedings 18th International Conference on Sciences and Techniques of Automatic Control and Computer Engineering (STA), Monastir, Tunisia, 21-23 December 2017, pp. 205-211.
146. Levi, E.; Bojoi, R.; Profumo, F.; Toliyat, H.A.; Wiliamson, S. Multiphase induction motor drives-a technology status review. IET *Elect. Power Appl*. **2007**, *1*, 489-516.
147. Barrero, F.; Duran, M.J. Recent Advances in the Design, Modeling, and Control of Multiphase Machines-Part I. *IEEE Trans. Ind. Electr.* **2016**, *63*, 449-458.
148. Frikha, M.A.; Croonen, J.; Deepak, K.; Benomar, Y.; El Baghdadi, M.; Hegazy, O. Multiphase Motors and Drive Systems for Electric Vehicle Powertrains: State of the Art Analysis and Future Trends. *Ener.* **2023**, *16*, 1-45.
149. Salomez, F.; Vienot, S.; Zaidi, B.; Videt, A.; Duquesne, T.; Pichon, H.; Semail, E.; Idir, N. Design of an integrated GaN inverter into a multiphase PMSM. In Proceedings 2020 IEEE Vehicle Power and Propulsion Conference (VPPC), Gijon, Spain, 18 November-16 December 2020.
150. Choi, H.-Y.; Park, S.J.; Kong, Y.K.; Bin, J.G. Design of multi-phase permanent magnet for slip propulsion. In Proceedings 2009 International Conference on Electrical Machines and Systems. Tokyo, Japan, 15-18 November 2009.
151. Duran, M.J.; Levi, E.; Barrero, F. Multiphase Electric Drives: Introduction. In Wiley, NJ, USA, **2017**, pp. 1-26.
152. Gerlach, M.E.; Zajonc, M.; Ponick, B. Mechanical stress and deformation in the rotors of a high-speed PMSM and IM. *e & i Elekt. und Infor.* **2021**, *138*, 96–109.
153. Chai, Y.; Li, Y.; Liang, P.; Pei, Y. Calculation of the Maximum Mechanical Stress on the Rotor of Interior Permanent-Magnet Synchronous Motors. *IEEE Trans. Ind. Electr.* **2016**, *63*, 3420–3432.
154. Gao, B.; Cheng, Y.; Zhao, T.; Sun, H.; Cui, S. A Review on Analysis Methods and Research Status of Hysteresis Motor. *Ener.* **2023**, *16*, 1-30.
155. Nasiri, A.A.; Mirsalim, M.; Nasiri, A.R. A Novel Hybrid Hysteresis Motor with Multi-Stack PM-Hysteresis Rotor; General Modeling, Analysis and Design Optimization. In Proceedings 2019 International Power System Conference (PSC), Tehran, Iran, 09-11 December 2019, pp. 150-158.
156. Al-Qarni, A.; EL-Refaie, A. Magnetic Gears and Magnetically Geared Machines with Reduced Rare-Earth Elements for Vehicle Applications. *World Elect. Veh. J.* **2021**, *12*, 1-23.
157. Wu, F.; El-Refaie, A.M. Permanent magnet vernier machine: a review. *IET Elect. Pow. Appl.* **2019**, *13*, 127-137.
158. Gerlach, M.E.; Zajonc, M.; Ponick, B. Mechanical stress and deformation in the rotors of a high-speed PMSM and IM. *Elektrot. & Inform.* **2021,** *138***,** 96-108.
159. Rasilo, P.; Audin, U.; Singh, D.; Martin, F.; Kouhia, R.; Belahcen, A.; Arkkio, A. Multiaxial magneto-mechanical modelling of electrical machines with hysteresis. In Proceedings 8th IET International Conference on Power Electronics, Machines and Drives (PEMD), Glasgow, UK, 19-21 April 2016.
160. Balluff, M.; Karthaus, J.; Schroder, M.; Gerlach, M.; Hameyer, K. Study on the Effects of Stator Segmentation on the Characteristics of an Electrical Vehicle Traction Drive. *e & i Elektrotechnik und Inform.* **2018**, *135*, 213–222.
161. Li, Y.; Chai, F.; Song, Z.; Li, Z. Analysis of Vibrations in Interior Permanent Magnet Synchronous Motors Considering Air-Gap Deformation. *Ener.* **2017**, *10*, 1-18.
162. Ebrahimi, B.M.; Roshtkhari, M.J.; Faiz, J.; Khatami, S.V. Advanced Eccentricity Fault Recognition in Permanent Magnet Synchronous Motors Using Stator Current Signature Analysis. *IEEE Trans. Ind. Electr.* **2014**, *61*, 2041-2052.
163. Borg Bartolo, J.; Degano, M.; Espina, J.; Gerada, C. Design and Initial Testing of a High-Speed 45-kW Switched Reluctance Drive for Aerospace Application. *IEEE Trans. Ind. Electr*. **2017**, *64*, 988–997.
164. Dresscher, D.; A. de Vries, T.J.; Stramigioli, S. Motor-gearbox selection for energy efficiency. In Proceedings IEEE International Conference on Advanced Intelligent Mechatronics (AIM), Banff, Canada, 12-15 July 2016, pp. 669-675.
165. Griffo, A.; Tsyokhla, I.; Wang, J. Lifetime of Machines Undergoing Thermal Cycling Stress. In Proceedings IEEE Energy Conversion Congress and Exposition (ECCE), Baltimore, USA, 29 September- 03 October 2019, 3831-3836.
166. Wu, F.; EL-Rafaie, A.M. Permanent magnet Vernier machines: A Review. In Proceedings XIII International Conference on Electrical Machines (ICEM), Alexandroupoli, Greece, 03-06 September 2018, pp. 372-378.

167. Toba, A.; Lipo, T.A. Genetic torque-maximizing design methodology of surface permanent-magnet vernier machine. *IEEE Trans. Ind. Appl.* **2009**, *36*, 1539-1546.
168. Chen, K.; Sarlioglu, B. Vernier Machine Analysis and Analytical Design for Traction Applications. In Proceedings International Aegean Conference on Electrical Machines and Power Applications (ACEMP) & International Conference on Optimization of Electrical and Electronic Equipment (OPTIM), Brasov, Romania, 02-03 September 2021.
169. Jafari, R.; Asef, P.; Ardebili, M.; Derakhshani, M.M. Linear Permanent Magnet Vernier Generators for Wave Energy Applications: Analysis, Challenges, and Opportunities. *Sustain.* **2022**, *14*, 1-35.
170. Tlali, P.; Wang, R.-J. Prospect of PM Vernier Machine for Wind Power Applications. *Ener.* **2022**, *15*, 1-26.
171. Li, J.; Wu, D.; Zhang, X.; Gao, S. A new permanent-magnet vernier in-wheel motor for electric vehicles. In Proceedings IEEE Vehicle Power and Propulsion Conference, Lille, 01-03 September 2010.
172. Zhao, F.; Kim, M.-S.; Kwon, B.-II.; Baek, J.-H. A Small Axial-Flux Vernier Machine With Ring-Type Magnets for the Auto-Focusing Lens Drive System. *IEEE Trans. Magn.* **2016**, 52, 8204604.
173. Faiz, J.; Amini-Valeshani, S.; Ghods, M. Design and performance of linear Vernier generators-The state of the art and case study. *Inter. Trans. Electr. Ener. Syst.* **2021**, *31*, 1-20.
174. Fernando, N.; Nutkani, l.U.; Saha, S.; Niakinezhad, M. Flux switching machines: A review on design and applications. In Proceedings 20th International Conference on Electrical Machines and Systems (ICEMS), Sydney, Australia, 11-14 August 2017.
175. Chen, H.; EL-Rafaie, A.M.; Demerdash, N.A.O. Flux-Switching Permanent Magnet Machines: A Review of Opportunities and Challenges-Part I: Fundamentals and Topologies. *IEEE Trans. Ener. Con.* **2020**, *35*, 684-698.
176. Chen, H.; EL-Rafaie, A.M.; Demerdash, N.A.O. A Review of Opportunities and Challenges-Part II: Design Aspects, Control, and Emerging Trends. *IEEE Trans. Ener. Con.* **2020**, *35*, 699-713.
177. Yue, Y.; Jia, S.; Liang, D. New Topologies of High Torque Density Machine Based on Magnetic Field Modulation Principle. *CES Trans. Elec. Mach. Syst.* **2023**, *7*, 1-10.
178. Gao, Y.; Liu, Y. Flux Reversal Machine Design. *Direct Torque Control Strategies of Electrical Machines*, Salem, F.B., Publisher: IntechOpen, 2021; pp. 1–172.
179. Ansari, A.A. A Review of Different Motor Types and Selection of One Optimal Motor for Application in EV Industry. *Inter. J. Electr. Pow. Engin.* **2022**, *16*, 1-7.
180. Siddiqi, M.R.; Yazdan, T.; Im, J.-H.; Humza, M.; Hur, J. Design and Analysis of a Dual Airgap Radial Flux Permanent Magnet Vernier Machine with Yokeless Rotor. *Ener.*, **2021**, **14**, 1-15.
181. Zhang, R.; Li, J.; Qu, R.; Li, D. Analysis and Design of Triple-Rotor Axial-Flux Spoke-Array Vernier Permanent Magnet Machines. *IEEE Trans. Ind. Appl.* **2018**, *54*, 244-253.
182. Kakihara, W.; Takemato, M.; Ogasawara, S. Rotor Structure in 50kW Spoke-Type Interior Permanent Magnet Synchronous Motor with Ferrite Permanent Magnets for Automotive Applications. In Proceedings IEEE Energy Conversion Congress and Exposition. Denver, USA, 15-19 September 2013, pp. 606-613.
183. Li, Y.; Pei, Y.; Song, Z.; Chai, F. Effect of rotor deformation on magnetic radial force in interior permanent magnet synchronous motors with V-shaped rotor structures. In Proceedings 42nd Annual Conference of the IEEE Industrial Electronics Society (IECON), Florence, Italy, 23-26 October 2016.
184. Rens, J.; Vandenbossche, L.; Dorez, O. Iron Loss Modelling of Electrical Traction Motors for Improved Prediction of Higher Harmonic Losses. *World Elect. Veh. J.* **2020**, *11*, 1-14.
185. Balamurali, A.; Kundu, A.; Li, Z.; Kar, C.N. Improved Harmonic Iron Loss and Stator Current Vector Determination for Maximum Efficiency Control of PMSM in EV Applications. *IEEE Trans. Ind. Appl.* **2021**, *57*, 363-373.
186. Riemer, B.; Lebmann, M.; Hameyer, K. Rotor design of a high-speed Permanent Magnet Synchronous Machine rating 100,000 rpm at 10kW. In Proceedings IEEE Energy Conversion Congress and Exposition, Atlanta, USA, 12-16 September 2010, pp. 3978-3985.
187. Shao, Y.; Wang, X.; Gao, Q.; Li, Y. Rotor Strength Analysis of Ultra-High Speed Permanent Magnet synchronous Motor. In Proceedings International Conference on Electrical Machines and Systems (ICEMS), Harbin, China, 11-14 August 2019.
188. Sakkas, G.K.; Kladas, A.G. Rotor deformation impact on operating characteristics of IPM Motor under High-Speed conditions. In Proceedings International Conference on Electrical Motor (ICEM), Valencia, Spain, 05-08 September 2022, pp. 8-13.